SANDIA REPORT
SAND2008-6162
Unlimited Release
Printed September 2008

Experiments for Foam Model Development and Validation

Lisa Mondy, Rekha Rao, Anne Grillet Douglas Adolf, Christopher Brotherton, Edward Russick, Raymond Cote, Jaime Castañeda, Kyle Thompson, Christopher Bourdon, Allen Gorby, Harry Moffat, Andrew Kraynik, and James Mahoney

Prepared by
Sandia National Laboratories
Albuquerque, New Mexico 87185 and Livermore, California 94550

Sandia is a multiprogram laboratory operated by Sandia Corporation,
a Lockheed Martin Company, for the United States Department of Energy's
National Nuclear Security Administration under Contract DE-AC04-94AL85000.

Issued by Sandia National Laboratories, operated for the United States Department of Energy by Sandia Corporation.

Available to DOE and DOE contractors from
U.S. Department of Energy
Office of Scientific and Technical Information
P.O. Box 62
Oak Ridge, TN 37831

Telephone: (865) 576-8401
Facsimile: (865) 576-5728
E-Mail: reports@adonis.osti.gov
Online ordering: http://www.osti.gov/bridge

Available to the public from
U.S. Department of Commerce
National Technical Information Service
5285 Port Royal Rd.
Springfield, VA 22161

Telephone: (800) 553-6847
Facsimile: (703) 605-6900
E-Mail: orders@ntis.fedworld.gov
Online order: http://www.ntis.gov/help/ordermethods.asp?loc=7-4-0#online

SAND2008-6162
Unlimited Release
Printed September 2008

Experiments for Foam Model Development and Validation

Lisa Mondy, Rekha Rao, Andrew Kraynik
Thermal and Fluid Processes

Harry Moffat
Nanoscale & Reactive Processes

Edward Russick
Organic Materials 1821

Douglas Adolf
Organic Materials 2453

Anne Grillet, Christopher Brotherton, Christopher Bourdon, Allen Gorby
Microscale Science & Technology

Raymond Cote, Jaime Castañeda
Thermal/Fluid Experimental Sciences

Kyle Thompson
Experimental Mechanics, Non-Destructive Evaluation, and Model Validation

Sandia National Laboratories
P.O. Box 5800
Albuquerque, New Mexico 87185-MS0346

James Mahoney
Advanced Engineering Simulation and Analysis
Honeywell Federal Manufacturing and Technologies, Kansas City Plant
P.O. Box 419159
Kansas City, Missouri 64141-6159

Abstract

A series of experiments has been performed to allow observation of the foaming process and the collection of temperature, rise rate, and microstructural data. Microfocus video is used in conjunction with particle image velocimetry (PIV) to elucidate the boundary condition at the wall. Rheology, reaction kinetics and density measurements complement the flow visualization. X-ray computed tomography (CT) is used to examine the cured foams to determine density gradients. These data provide input to a continuum level finite element model of the blowing process.

ACKNOWLEDGMENTS

The authors would like to acknowledge very helpful discussions with David Noble (1514), Jim Aubert (1821), Sara Leming (1521), Jeremy Lechman (1516), Carlton Brooks (1513), and Mike Gerding (KCP). We are especially grateful to Wayne Trott (1512) for thermocouple calibration.

CONTENTS

FIGURES

TABLES

1. INTRODUCTION

Foam encapsulation provides protection from shock, vibration, and thermal influences for a wide variety of electro-mechanical weapon components. Use of foam provides a good compromise between the need for this protection and the requirement to be light weight. Because the encapsulation occurs near the end of the manufacturing process, expensive components (e.g., a firing set may cost $150K) are at risk if the encapsulation is flawed. Unfortunately, the foam processing, involving a polymerizing, multiphase material with changing microstructure, is difficult to understand and predict. Sandia's Advanced Simulation and Computing (ASC) program is developing a computational model to provide guidance early in the design process to optimize the hardware for foam encapsulation. The Campaign 6 Foam Processing Project has provided experimental data as input to, as well as validation of, Sandia's foam modeling effort, the development of which is an ASC Level II milestone for September of 2008. Our experiments also provide significant insights into possible Kansas City Plant (KCP) process improvements.

Blown epoxy foams are used for many encapsulation applications at Sandia to stabilize and protect critical components. These foams are manufactured from a two part epoxy mixture that has been seeded with a blowing agent. The blowing agent's role is to evaporate during processing to create the large void fraction within the foam. For Sandia's applications, we are interested in physically blown foam that starts as an emulsion of Fluorinert™ blowing agent droplets in epoxy monomer and curative, which is then injected into a hot mold to boil the Fluorinert and produce foam in situ. Model development has required experimental studies of a physically blown epoxy foam to supply property values needed as input to the model, boundary conditions for model calculations, and data for validation of model predictions. Although the foam of most interest is the Removable Epoxy Foam (REF), in this work we have used primarily EFAR20 to represent a typical epoxy foam and have collected only limited data using REF308 due to lack of material availability.

Observations of the foam blowing process in a simple channel were used to determine density vs. time and density vs. temperature and time mathematical models. Microfocus video was used in conjunction with particle image velocimetry (PIV) to elucidate the boundary condition at the wall. In addition, the heat and rate of the polymerization reaction were determined using Differential Scanning Calorimetry and correlated with rheological measurements of the epoxy continuous phase. Rheology of the foam itself was measured and related to the gas volume fraction. These data were used in the development of first and second generation computational models in the Sandia High Performance Computing molecular dynamics code, ARIA, simplified so that they could be used in complex geometries. These experiments provided input to the model and are discussed in the next section.

Looking forward to future more complete models, we have also examined the nucleation process and have shown that the air incorporated into the unfoamed epoxy during mixing plays a major role in the nucleation of the boiling of the blowing agent. Both mixing studies and single bubble/droplet studies are discussed in the third section.

Finally, we have observed EFAR20 rising in a mold designed by Kansas City personnel originally for use as a quality assurance tool. The Kansas City mold was duplicated at Sandia and temperature instrumentation was added. Video allowed quantitative measurement of the foam volume and front location. The cured foam was then examined with x-ray computed tomography (CT) to determine density gradients. These validation studies are described in the fourth section.

2. EXPERIMENTS TO OBTAIN MODEL INPUT DATA

2.1. Foam Rise in a Channel

In order to create a preliminary engineering model of the foam rise, we decided simply to assign a rise rate to the foam based on empirical measurements of foam free-rise self-expansion in a channel. The material used was EFAR20, a nominally 20 pound per cubic foot (pcf) epoxy foam made up of Part A, Epon™ 828 and Epon™ 8121 (Shell) resins, and Part B, a mixture of amine curative agents (Shell Epi-Cure® and Air Products Ancamine® 2049), Cab-O-Sil® (Cabot Corp.) particles, silicone surfactant Dabco® DC193 (Air Products), and the Fluorinert™ FC-72 (3M) blowing agent. The precursor epoxy materials were mixed in a manner close to that used in the actual encapsulation process, with the exception that Part B was heated slightly (to 40°C) in tightly closed containers and shaken with a paint shaker for 5 minutes and then allowed to return to room temperature before each experiment. This was done to minimize some clumping of the Cab-O-Sil that we thought we were observing.

In actual encapsulation processes, Part A is preheated to just below the boiling point of Fluorinert. In Albuquerque, we used 50°C, based on the manufacturer's value of the boiling point of 53°C at 12 psia (a typical ambient pressure at the altitude of Albuquerque). Immediately before an experiment, Part B was shaken again on the paint shaker for one minute at ambient temperature (typically 21°C). Next, Part B was mixed into the preheated Part A by hand, vigorously stirring for one minute. Nominally 20 g of the mixture was loaded into a syringe, its mass measured, the plunger location marked for a volume measurement, and then the material was injected into the preheated mold held in an oven. Tests at mold and oven nominal temperatures of 54°C, 60°C, 63°C and 66°C were performed.

The oven was modified by replacing the door with a clear glass cover to allow filming of the foam rise. Unfortunately, this was somewhat detrimental to the ability of the oven to control a steady temperature. Figure 1 shows that the oven temperature cycles and drifts over time. The temperature was nonetheless controlled to approximately ±1.0°C.

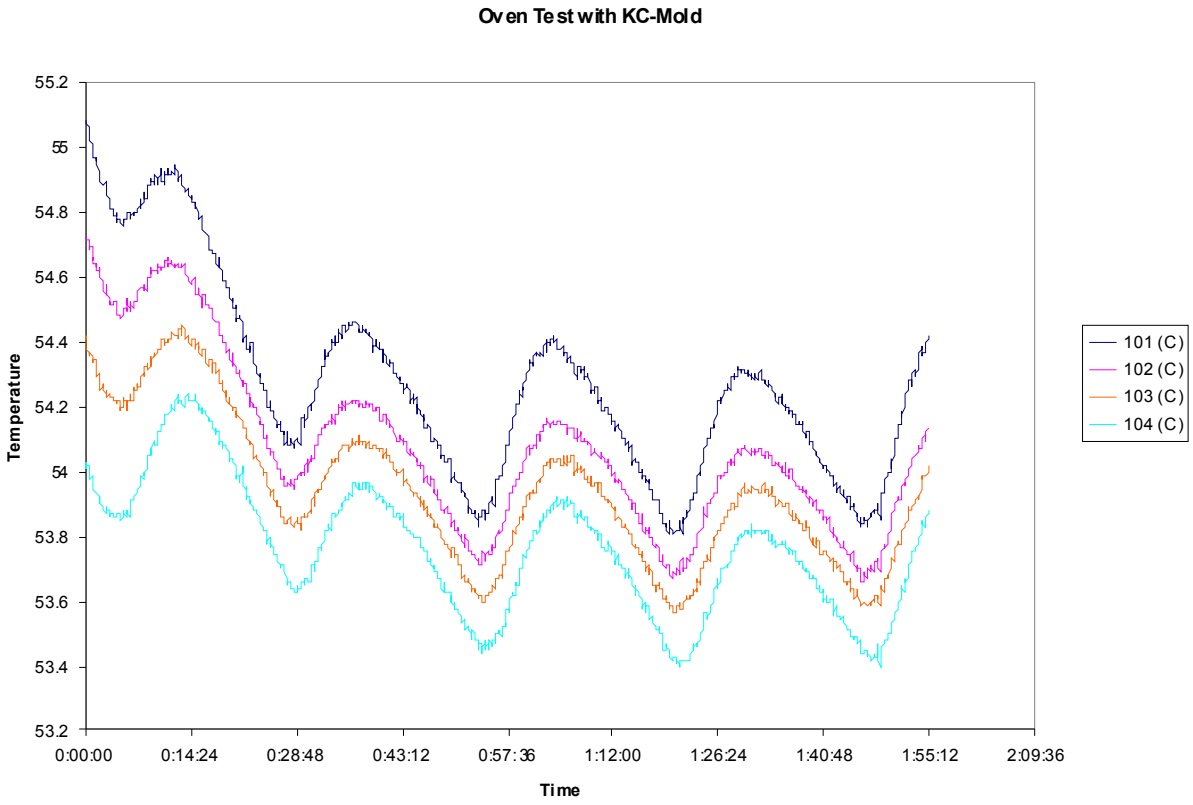

Figure 1. The oven temperature cycles and drifts over a two hour period. Numbers in the legend indicate thermocouple number corresponding to the thermocouples listed in Figure 31.

Experiments were performed in narrow slots so that the foam would heat up quickly and the foam temperature would, therefore, be as uniform as possible during the experiment. The channel was a 0.64 cm deep, 1.27 cm wide, 20.3 cm high (0.25”×0.5”×8”) slot in an aluminum block with an acrylic glass cover held in front (Figure 2). Three camera views were used, as also shown in Figure 2. The expanded view was used to calculate the height vs. time of the foam, and the close-up views were used to examine the details of the foam structure and for particle image velocimetry (PIV) to obtain slip velocities (see Section 2.2).

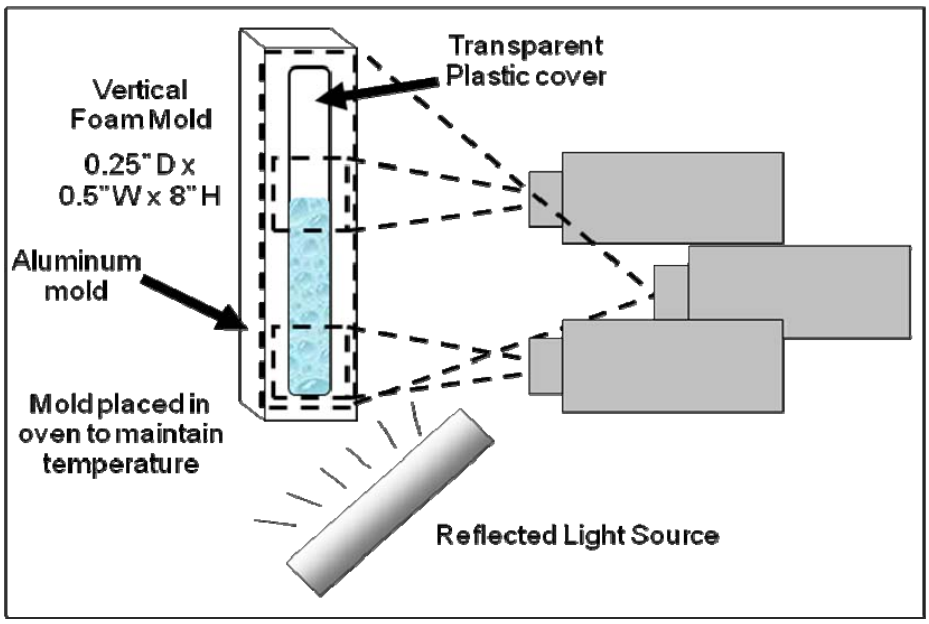

Figure 2. Schematic of experimental equipment.

The cameras recorded video at 30 frames/second. Individual frames from two cameras (not the PIV camera) for the foam at various times can be extracted from the video, as shown in Figure 3. Knowing the frame number and frame rate, one can determine the elapsed time. From the known geometry of the channel, the measured height of the foam column, and the known amount of liquid injected, the foam density can be quickly estimated assuming that the change in volume is caused by the gas evolution with negligible loss of liquid volume from the liquid due to evaporation of the Fluorinert, which comprised approximately 3% of the volume of the liquid.

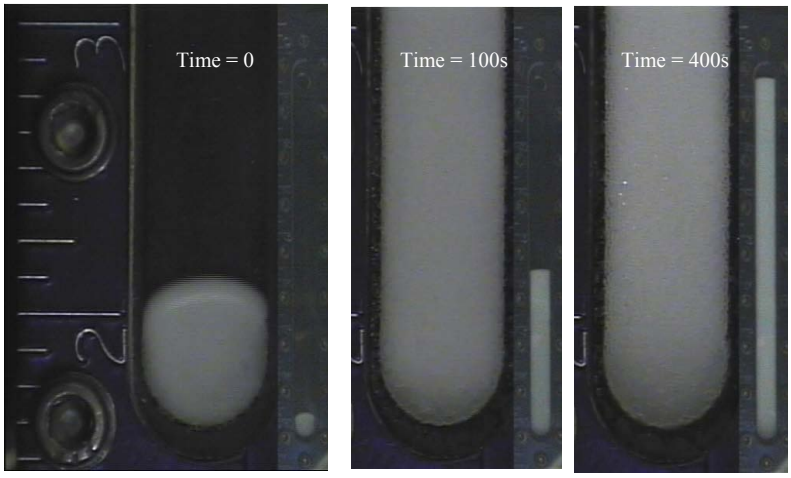

Figure 3. Partial images from a foam rise experiment.

Temperature at the inlet and the ambient pressure were recorded. A more exact measure of gas evolution correcting for the loss of liquid volume, as well as the change in temperature and

pressure, was considered unnecessary because of larger uncertainties in the analysis of these data. Although we want to set time = 0 to be when the foam injection has ended, there was some uncertainty in this actual time, because in these early tests we did not create a timing mark on the film when the injection stopped. If one knew the initial density of the material, the height at which the material was completely injected could be calculated from the measured mass of material. Unfortunately, because the foam is expanding immediately as it enters the hot mold, it is difficult to know the density and, hence, the height at time = 0. Furthermore, although we know the density of the mixture of liquid components alone is 1.14 g/cm^3 (as can be calculated from the information in Table 1), mixing incorporates a significant amount of air. Measurements of the volume of the syringe and the mass injected indicate that a typical initial density is close to 0.9 g/cm^3. This value agrees with that obtained in separate experiments in which the foam was mixed in a volume-calibrated beaker.

Table 1. Epoxy Foam Formulations Used in This Study

Material	Weight fraction	Density (g/cm^3)
EFAR20		**1.14 (Unfoamed)**
EFAR20 Part A (resin)	*0.654*	*1.17*
• Epon™ 828 resin	• 0.6	• 1.17
• Epon™ 8121 resin	• 0.4	• 1.17
EFAR20 Part B (curative)	*0.346*	*1.08*
• Ancamine® 2049 curing agent	• 0.585	• 0.95
• Epi-Cure® 3270 curing agent	• 0.245	• 0.97
• Dabco® DC-193 surfactant	• 0.019	• 1.07
• Cab-O-Sil® M-5 fumed silica	• 0.019	• 2.20
• Fluorinert™ FC-72	• 0.132	• 1.7
REF308		**1.23 (Unfoamed)**
REF308 Part A (resin)	*0.627*	*1.19*
• Removable epoxy resin 1 (RER1)	• 0.48	• 1.2, approximately
• Removable resin 2 (RR2)	• 0.12	• 1.2, approximately
• Epon™ 8121 resin	• 0.40	• 1.17
REF308 Part B (curative)	*0.373*	*1.23*
• Ancamine® 2049 curing agent	• 0.361	• 0.95
• Ancamine® 2205 curing agent	• 0.142	• 1.04
• Dabco® DC-193 surfactant	• 0.069	• 1.07
• Cab-O-Sil® M-5 fumed silica	• 0.009	• 2.20
• Fluorinert™ FC-72	• 0.419	• 1.7

Figure 4 shows the sensitivity of the calculated foam density to the value assumed for the initial density. The data depicted here were taken in a 54°C oven. For mass balance reasons, it could be preferable to ignore the incorporated air and assume an initial density of 1.14 g/cm^3 in the computational model. One can see from Figure 4 that the assumed initial density affects the final density very little.

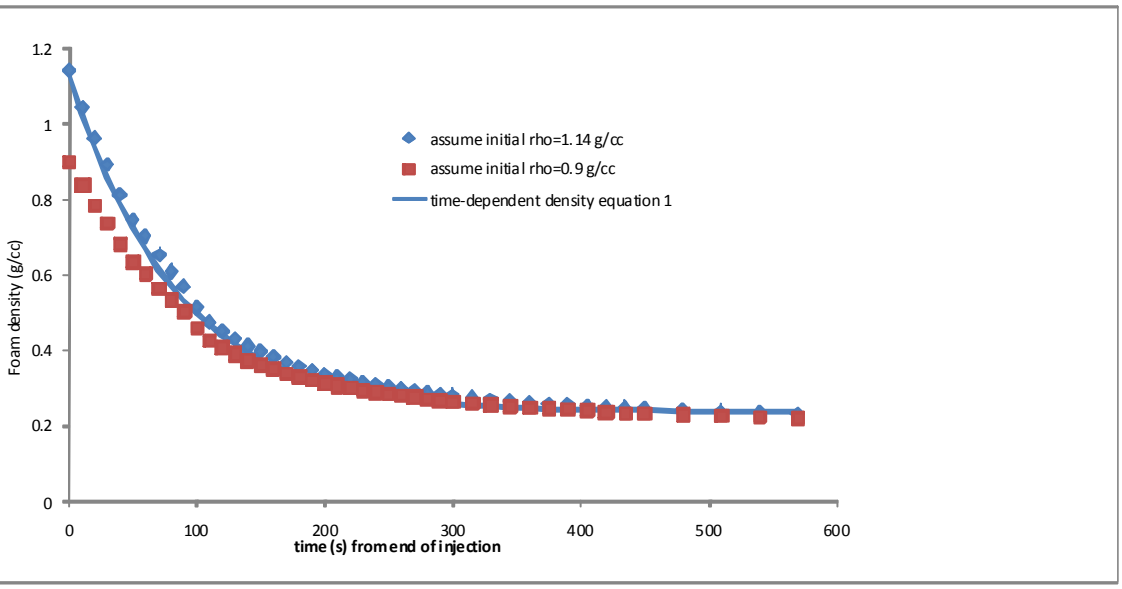

Figure 4. Typical data representing the change in foam density with time as it expands with a nominal oven temperature of 65°C.

From the data in Figure 4, and following Seo and Youn [Seo and Youn 2005], we develop a simple time-dependent density model:

$$\rho = \rho_f + (\rho_i - \rho_f)e^{-kt}, \tag{1}$$

where ρ_i is the initial density, taken to be 1.14 g/cm^3 here, ρ_f is the final density, which in this series of experiments was typically 0.24 g/cm^3, and time constant k, obtained by fitting Equation 1 to the data shown in Figure 4, is 1/80 s^{-1}.

Within the range of the temperatures tested, as the temperature increases, the foam rises faster. Preliminary foam rise data were taken in a similar fashion as described above, but with less control of the initial quantity of material injected into the slot and, in some cases, less temperature monitoring. However, these first measurements were taken over a higher range of oven temperatures. By considering both the preliminary data set and the subsequent more controlled data , including all the various temperatures, one can modify Equation 1 to include the effects of temperature. Figure 5 documents the density changes at three oven temperatures, assuming that the initial density was 1.14 g/cm^3. Also shown in Figure 5 is a fit to preliminary data in a more complicated fashion to take into account the effects of temperature and based on the nominal oven temperature only.

$$\rho = (\rho_i - \rho_f)\exp\left[\frac{-(t-t_i)}{\frac{A}{T} - B}\right] + \rho_f . \tag{2}$$

Here, ρ_f was taken to be 0.27 g/cm^3, the value typically measured in this series of experiments. T is the temperature in Kelvin. Fitting Equation 2 to the data in Figure 5 resulted in values for the parameters, A and B, of 116250 K s and 274.26 s, respectively. An actual temperature of the foam was recorded for each data point in Figure 5, so the calculated points here take into account the temperature history in this case.

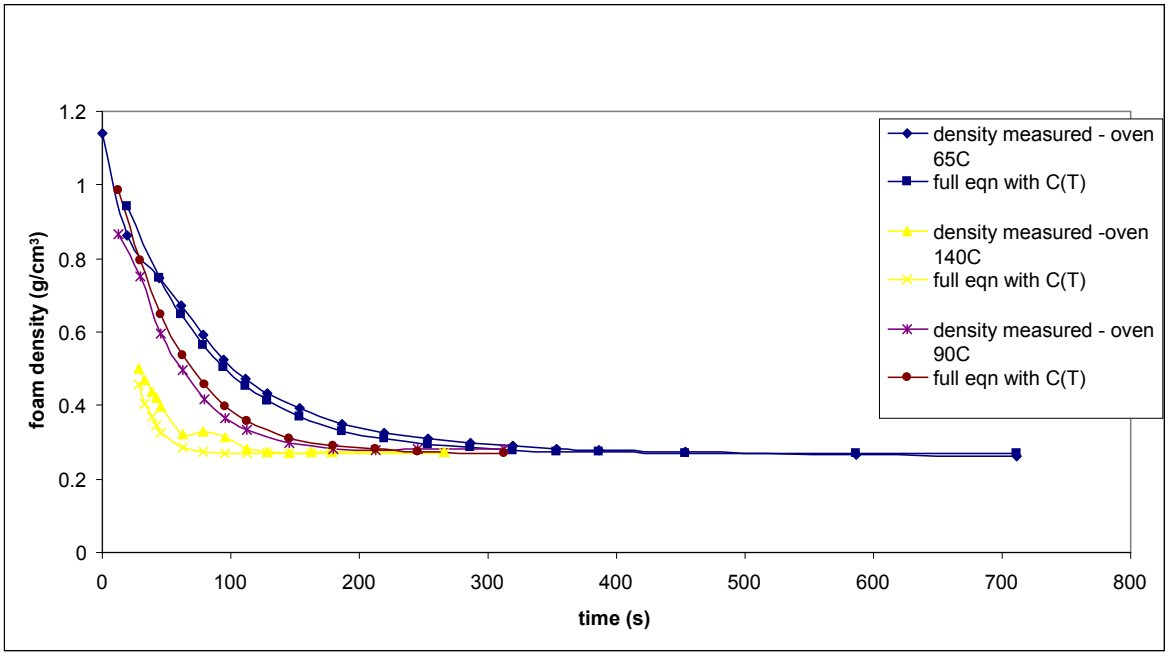

Figure 5. Foam density evolution as measured in original experiments at various temperatures, compared to Equation 2 with C(*T*)=*A*/*T*-*B*.

Figure 6 shows the more recent data at both 54°C and 66°C nominal oven temperatures compared to the time-temperature-density model originally developed with the earlier data, Equation 2, and calculated using the temperature history data. Also plotted are the data at the lower temperature assuming that the initial density is the liquid density (ρ_i = 1.14 g/cm^3). Here, the equations ignore the incorporated air and go to a final density of 0.24 g/cm^3.

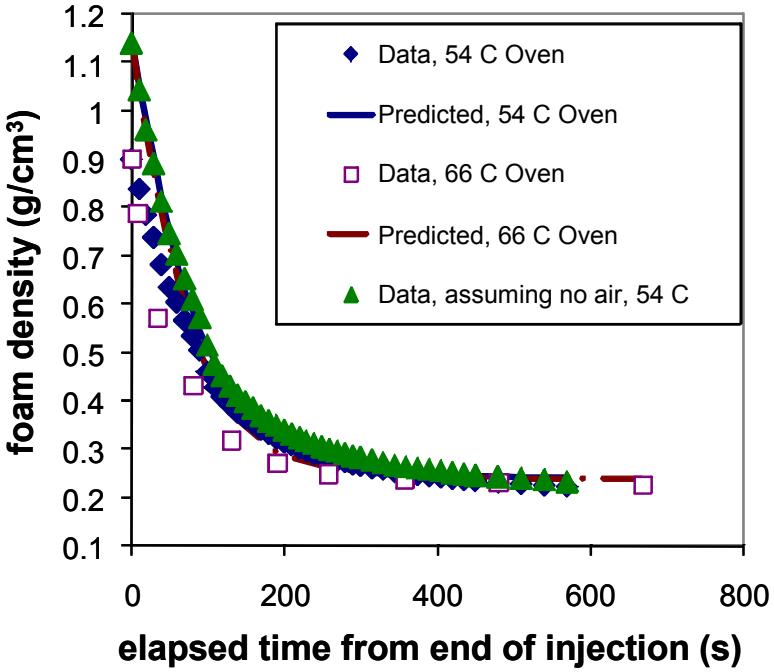

Figure 6. Foam density evolution at two temperatures.

In an attempt to measure the foam rise in a truly isothermal experiment, we proposed to inject the foam mixture at a high pressure (nominally 30 psia) and hold it at this pressure to suppress the boiling of Fluorinert while the material came to a steady temperature. The concept is similar to that discussed in Section 3, following. However, we found that the foam did not rise in the same manner as it did when injected at ambient pressures. Figure 7 shows the difference in the resulting foam height after a two minute hold at 30 psia. Because the resulting foam was quite different than that expected in the real encapsulation process, the data taken in this manner was not used for the modeling. These data did, however, add to the evidence that air incorporation is critical for EFAR to rise. This will be discussed in detail in Section 3.

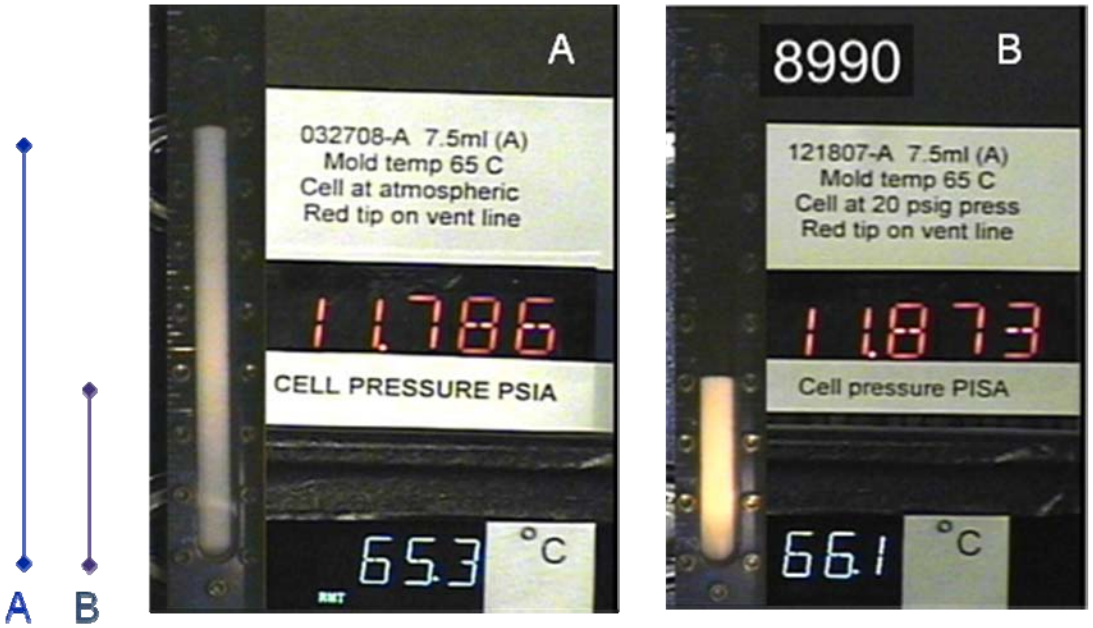

Figure 7. Holding the pre-foamed epoxy mixture for two minutes until a constant temperature was reached resulted in a much denser foam (B, right).

2.2. PIV to Determine Slip Boundary Conditions

While we were obtaining height vs. time data, we also obtained detailed measurements of the velocity of the foam adjacent to the transparent wall by using particle image velocimetry (PIV). Tracer particles were not necessary since the foam bubbles themselves could be used for data analysis. Images were taken at 1-second intervals with a CoolSnap™ EZ CCD camera using standard optics. PIV was performed using DaVis *(Da*ta Quality *Vis*ualizer) visualization software to cross-correlate successive images. By the time the foam reached the view of the PIV camera (Figure 2), it had an average gas volume fraction of about 0.5. By the time we stopped filming for PIV, the foam had an average gas volume fraction of about 0.71.

Figure 8 illustrates a typical foam experiment at two separate time points. On the left is a close-up of a rising foam interface with superimposed velocity vectors results from PIV. As the foam fills the mold, the interface flow profile is fountain-like. However, it should be noted that there is a small gap between the transparent wall and the rest of the mold that contributes to the interface flow profile. On the right of Figure 8 is an image at a later time illustrating the foam motion within the mold. At this time point, the volume fraction of the gas in the foam is ~0.60, and the PIV results show a slip velocity along the mold wall. The velocity profile consists of two separate regions—a shear velocity profile near both side walls, and a plug flow velocity

profile near the center. From this image, it is also possible to see the gradient in the vertical velocity along the direction of flow.

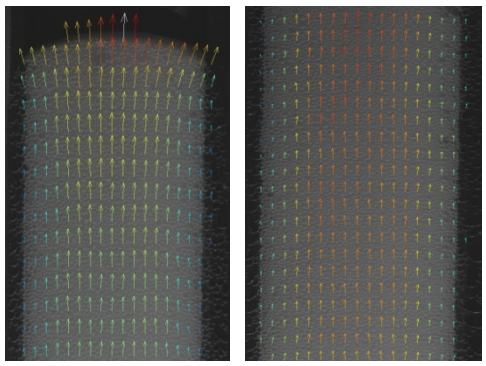

Figure 8. Particle image velocimetry of the rising foam interface (left) and the foam motion at a later time (right).

Figure 9 shows a typical foam velocity profile for six distinct time points. As time increases, the available blowing agent decreases, the viscosity increases and the volume fraction increases resulting in a decrease in the average slip velocity, but the profile maintains the two flow regions. During the experiment, the volume fraction of gas is determined from the height of the sample and the known quantity of liquid injected. The unblown foam has density of ~1.1g/cm^3, and the final density is ~0.3 g/cm^3, which corresponds to a final gas volume fraction of ~0.73.

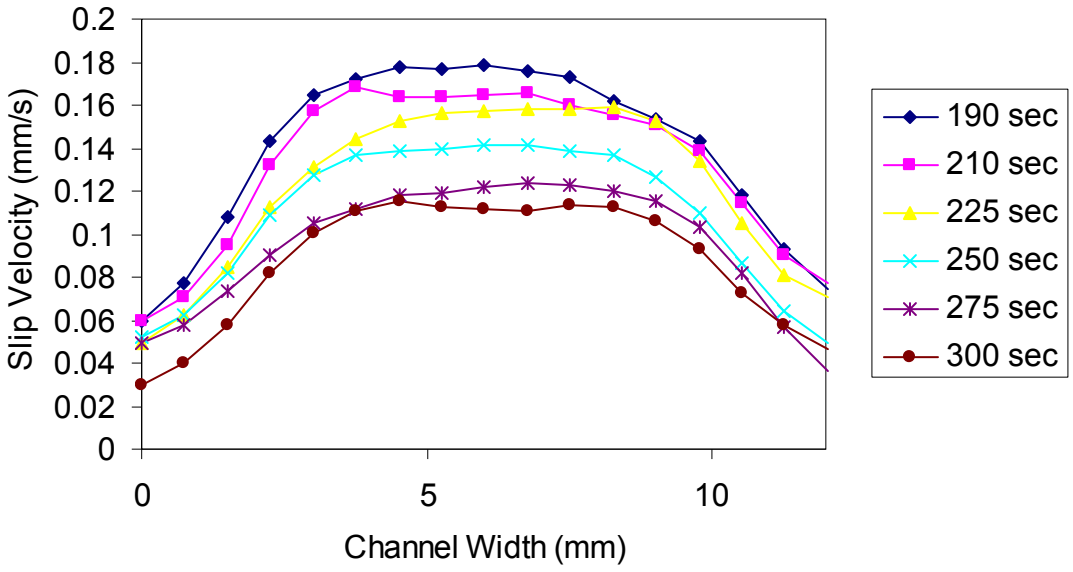

Figure 9. Free rise slip velocity versus mold width for six distinct time points.

Figure 10 shows the slip coefficient (β) versus foam viscosity for three temperatures. The slip coefficient is defined as [Kraynik 1988]:

$$\beta = \frac{v_y(x=0)}{\mu\left(\frac{dv_y}{dx}\right)_{x=0}}, \tag{3}$$

where $v_y(x = 0)$ is the slip velocity of the foam adjacent to the mold wall (measured using PIV), μ is the viscosity of the continuous phase (see next section) and (dv_y/dx) is the gradient of the velocity at the wall. The maximum velocity of the foam (away from the walls) was determined from the height vs. time measurements discussed previously. The velocity next to the walls was assumed to be that measured with PIV. The velocity gradient adjacent to the wall was determined by fitting the foam velocity profile to a parabola, from the maximum velocity away from the walls to the slip velocity at the wall, and taking the derivative. The above slip coefficient definition assumes a Newtonian continuous phase, which is valid for this foam system at early times before significant polymerization has taken place. Over the foam viscosity range under investigation, the slip coefficient is relatively constant, which provides further evidence that the continuous phase can be considered Newtonian. The data also suggest that the slip coefficient has a slight dependence on temperature. However, due to the variability of the foam starting components, the temperature effect could be attributed to subtle differences in the foam materials. Given these considerations, the slip coefficient is 0.00068 ± 0.00023 cm^2 s/g and is valid over the range of the conditions investigated.

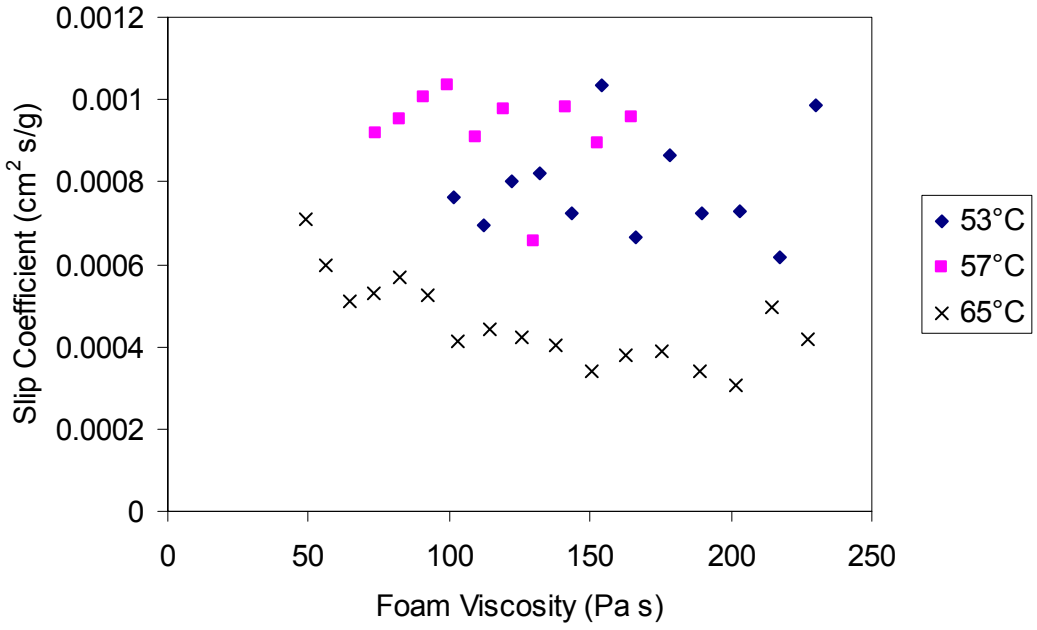

Figure 10. Slip coefficient versus foam viscosity for three temperatures.

2.3. Reaction Kinetics and the Viscosity of the Continuous Phase

2.3.1. EFAR20

The continuous phase viscosity is needed for the computational model, as well as the slip calculations. However, although we estimated the viscosity change to be small over the time of the PIV measurements, in general this property is a function of the extent of the reaction and the temperature. In turn, the extent of reaction is also a function of time and temperature. Differential Scanning Calorimetry (DSC) was used to determine the heat of reaction and approximate the extent of reaction with time and temperature for the reacting epoxy, the continuous phase of the foam. The methodology was established to correlate the viscosity of the materials with the extent of reaction and, hence, time and temperature history.

DSC data were collected at various temperatures and are shown in Figures 11-13. As shown in Figures 11 and 12, the heat flow measurements at different temperatures overlay when shifted, indicating only one reaction mechanism. The amount of the shift reveals the activation energy, E_a, is 11 kcal/mol. The reaction is exothermic, with an average heat of reaction of 250 J/g.

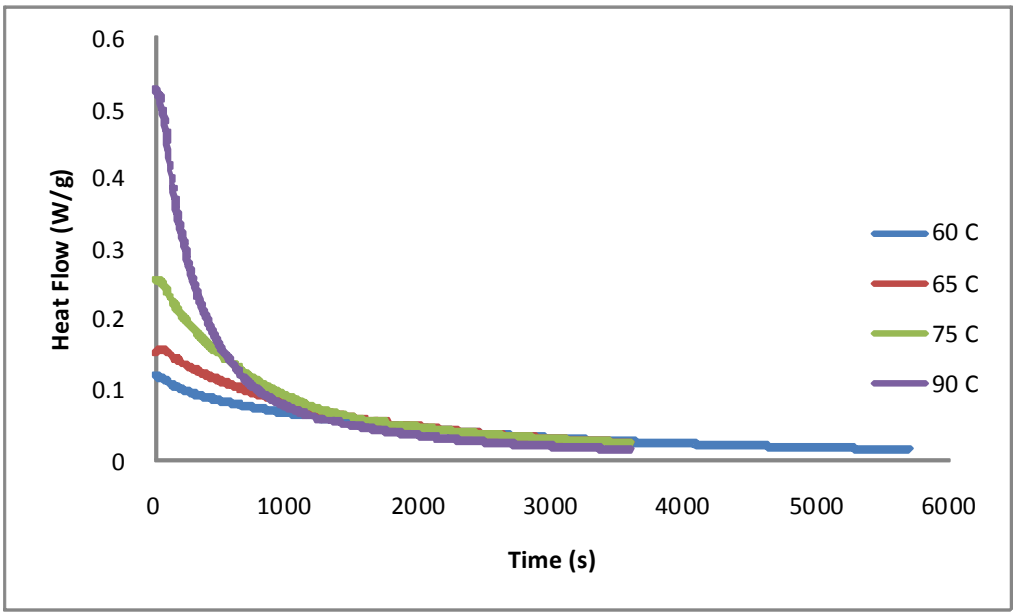

Figure 11. Raw DSC data.

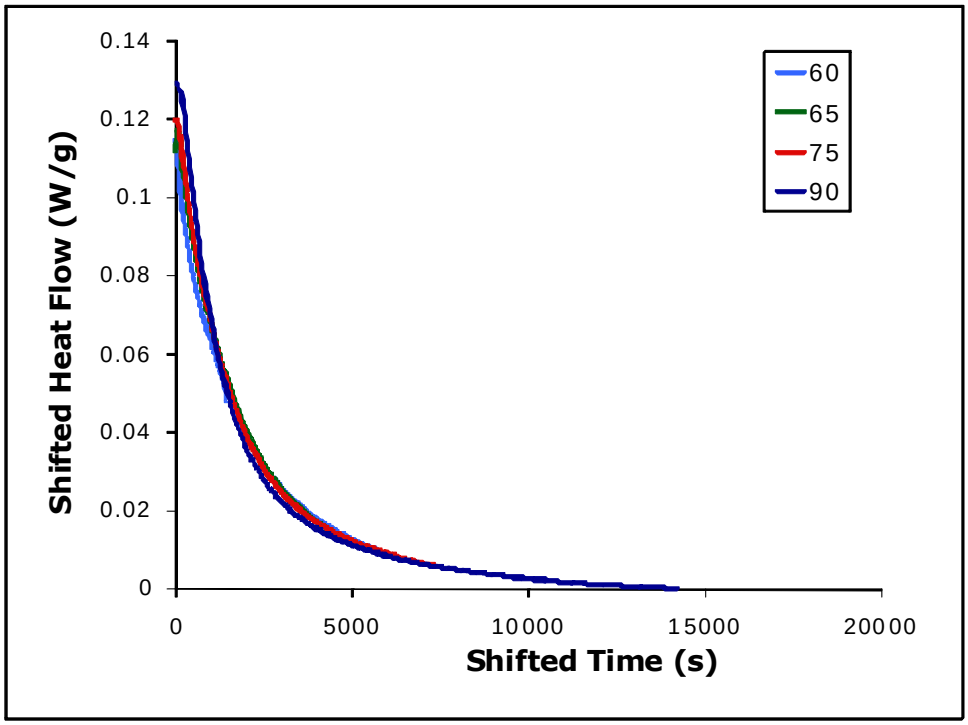

Figure 12. Shifted DSC Data.

The data in Figure 12 can be integrated over time and normalized by the heat of reaction to yield the extent of reaction. While cross-linking of reacting epoxy is a highly complex process, it generally follows condensation chemistry in which a general kinetics equation can describe the reaction rate in terms of the extent of reaction ξ, in the general form [Adolf et al. 1996, 1997a, 1997b]:

$$\frac{d\xi}{dt} = k_0(k_1 + k_2\xi^m)(1-\xi)^n, \qquad k_0 = ke^{\frac{-Ea}{RT}} \tag{4}$$

In the case of EFAR20 the extent of reaction ξ, is found to fit a simpler form:

$$\frac{d\xi}{dt} = ke^{-E_a/RT}(1-\xi)^n, \tag{5}$$

where the value obtained for k is 8.60×10^3 s^{-1}, the value for n is 1.4 (dimensionless), T is the temperature measured in Kelvin, and R is the gas constant: 1.987 cal/(mol K). Figure 13 shows the measured and predicted extent of reaction using this model.

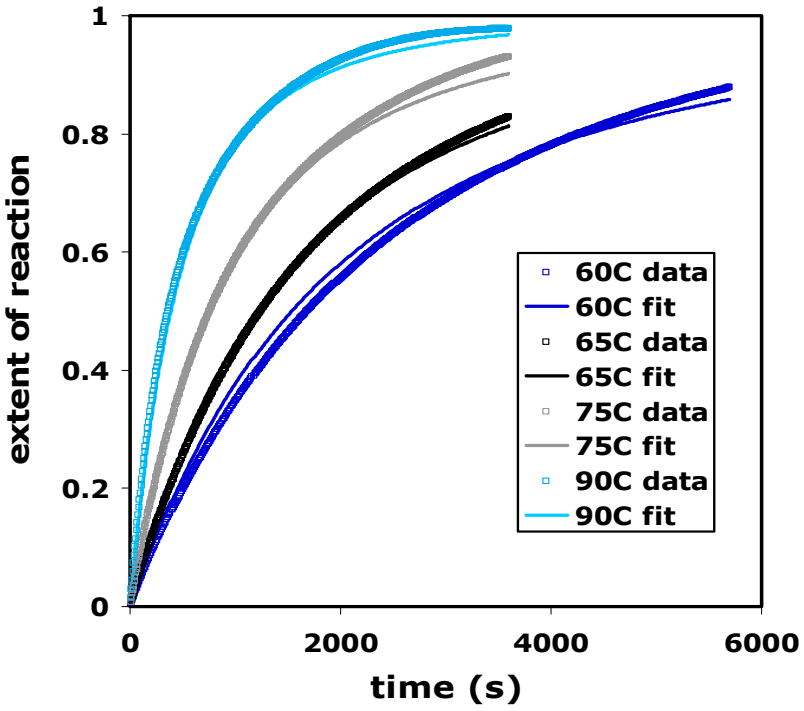

Figure 13. Extent of reaction at various temperatures.

For each temperature tested with the DSC, rheological data were taken in a parallel plate geometry at a steady shear rate of 2 s^{-1}. The epoxy did not show a significant effect of shear rate during the early times of interest. Figure 14 shows the measured viscosity with time. The continuous phase viscosity η can be written as a arbitrary function of temperature, T and extent of reaction, ξ. It appears that these effects operate independently such that:

$$\eta = \eta_0 \, f(T) \, f(\xi), \tag{6}$$

where η_0 is the proportionality constant. For operating temperatures far above the current glass transition temperature of the reacting epoxy, the temperature dependence can be modeled accurately by an Arrhenius relationship [Ferry 1980]:

$$f(T) = e^{E_\eta / RT}, \tag{7}$$

where E_η is the viscosity activation energy, R is the gas constant, and T is the absolute temperature. The shear thinning behavior at lower shear rates and higher gas volume fractions will be ignored. Dynamic percolation theory [Martin, Adolf, and Wilcoxon 1989] predicts a dependence of the Newtonian viscosity on extent of reaction with the form:

$$f(\xi) = \left[\frac{\xi_c^z - \xi^z}{\xi_c^z} \right]^{-x}, \qquad (8)$$

where ξ_c^z is the extent of reaction at the gel point.

Therefore, again shifting the data to a single curve could be accomplished, using a value of E_η of 13 kcal/mol. Figure 15 displays the predicted viscosity fit to the form of Equations 6-8:

$$\eta = \eta_0 e^{E_\eta / RT} \left(\frac{\xi_c^z - \xi^z}{\xi_c^z} \right)^{-x}, \qquad (9)$$

where the pre-exponential factor η_0 is 4.00×10^{-9} Pa s, ξ_c is the extent of reaction at the gel point for which a value of 0.6 was obtained, z is 1.0, and dimensionless fitting parameter x is 3.5. The fit was performed so that the region of most interest, 65°C, was best predicted, as shown in Figure 16, which compares the data to the prediction of Equation 9.

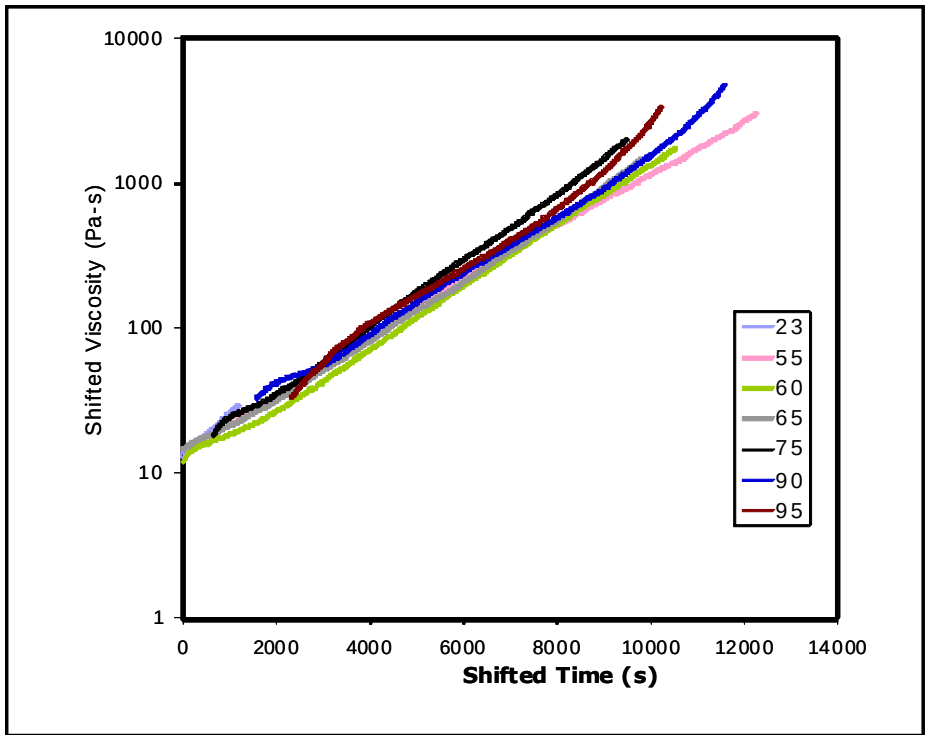

Figure 14. Measured viscosities at various temperatures (°C), shifted to overlay.

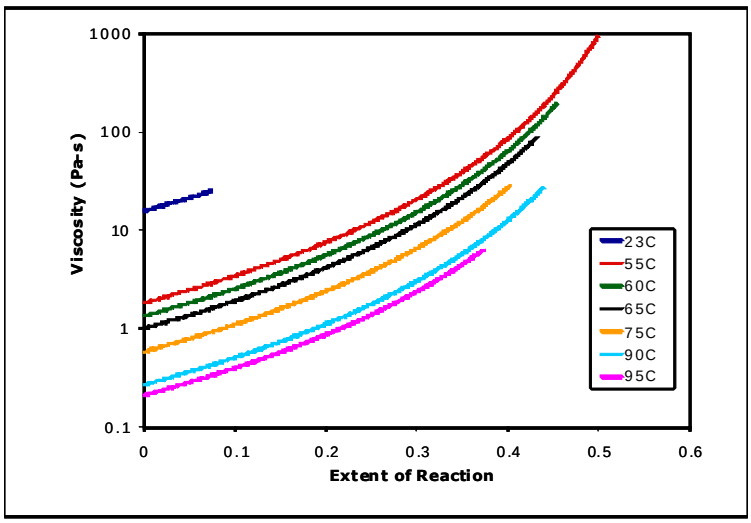

Figure 15. Viscosity dependence on extent of reaction as calculated with Equation 9.

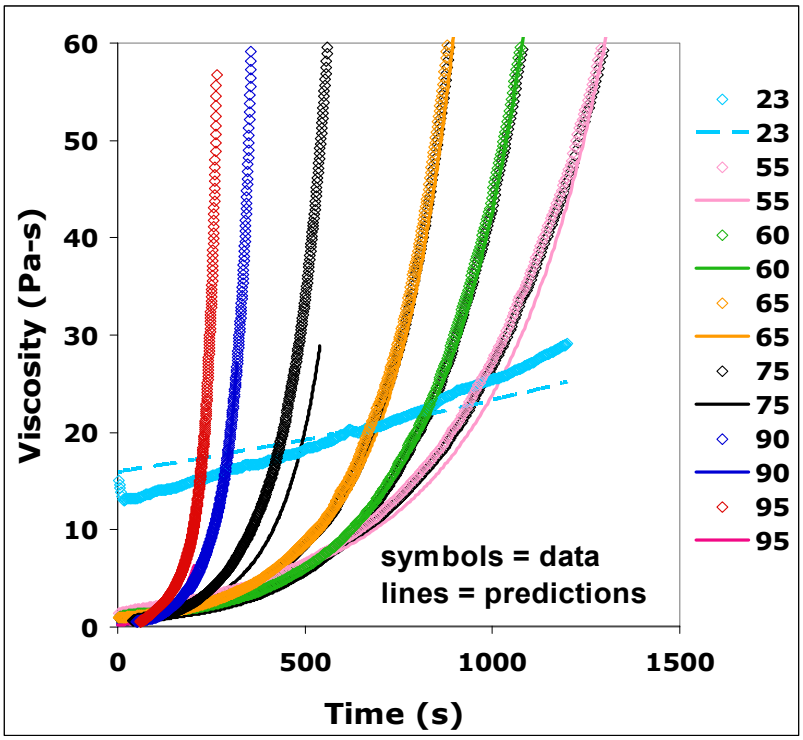

Figure 16. Measured viscosities compared with predicted viscosities from Equation 9.

2.3.2. REF308

In addition to the viscosity measurements for the EFAR20 continuous phase, we also tested REF308. Figure 17 shows the measured extent of reaction compared to that predicted by Equation 4, when E_a is 7 kcal/mole, k is 150 s^{-1}, k_1 is 0.28, k_2 is 1, m is 2, and n is 2.4.

The REF308 viscosity was fit to the form of Equation 9 (figure 18) in a similar manner to that described for EFAR20. The best fit values for the parameters follow: η_0 is 40 Poise, E_η is 0 kcal/mole, z is 0.5, x is 2, and ξ_c is 0.65. The viscosity starts higher than that of the EFAR20 and increases faster because of a rapid cure. The heat of reaction for the polymerization of REF308 is 134 J/g.

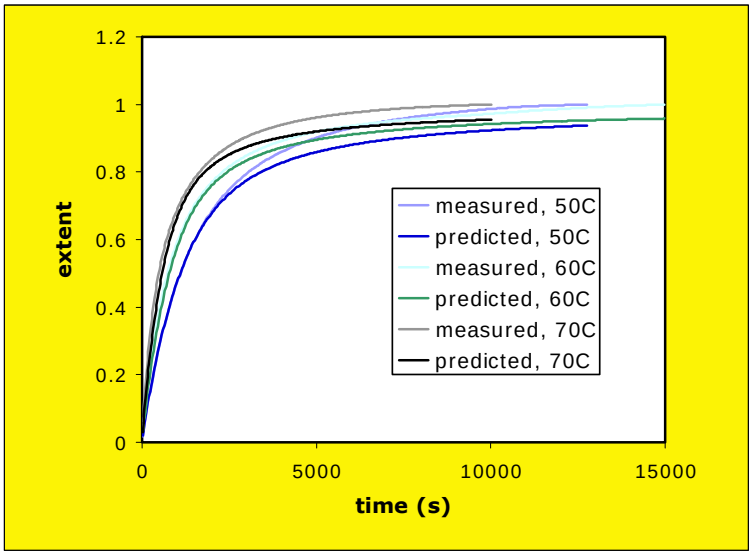

Figure 17. Extent of reaction of REF308.

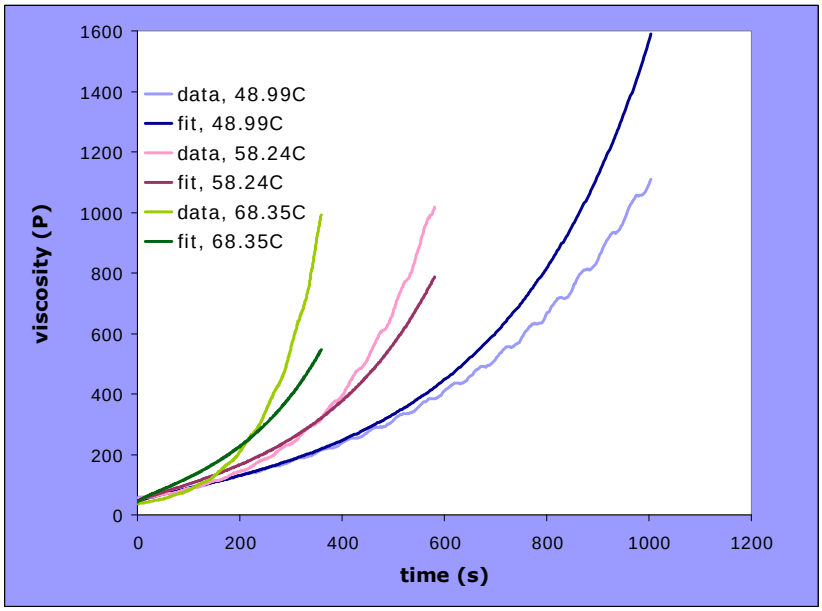

Figure 18. Viscosity for REF308.

2.4. Foam Rheology

The foam viscosity is needed for the foam model flow calculations. We expected the foam viscosity η_f to be a strong function of the gas volume fraction ϕ_g [Prud'homme and Khan 1995] in the form:

$$\eta_f = \eta \exp\left(\frac{\phi_g}{1-\phi_g}\right) \tag{10}$$

To determine if this was a satisfactory approximation to the foam effective viscosity, we tested the EFAR20 as it was foaming in a shear rheometer using a parallel plate geometry. Because the foam was expanding during the test, the foam escaped out the side of the parallel plates and, therefore, the volume of the sample did not change, but the density of the sample did. Both quantities are needed for the interpretation of the viscosity measurement. We used a temperature ramp in the rheometer that mimicked that of the free-rise experiments (Figure 19). Knowing that the viscosity of the foam would be sensitive to cell breakage, we tested a shear rate as low as possible given the resolution of the torque sensor in the rheometer. We also measured the dynamic viscosity in small amplitude oscillations to try to measure viscosity while minimizing cell breakage. Unfortunately, fluids with structure, like foams, do not follow Cox-Merz rules relating dynamic and shear viscosities. Nevertheless, the lowest shear rate measurements agreed reasonably well with the oscillatory measurements at low frequencies, giving us more confidence in these low shear rate results.

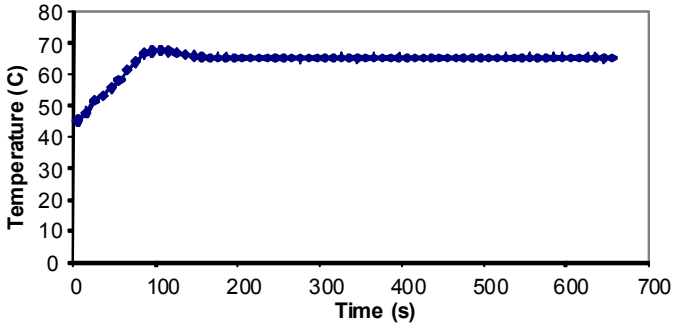

Figure 19. Temperature ramp in the free-rise experiment used to predict gas content.

Figure 20 describes the results of the rheometry tests, and shows the growth of the viscosity with time (as the foam gas fraction increases and the density decreases). The foam appears to be shear thinning, which is typical for these materials. However, as the shear rate increases, the foam structure is undoubtedly damaged, so, at a constant gas fraction, it will appear not only shear thinning but time-dependent. Nevertheless, we will interpret the low shear rate data as if the viscosity is only a function of the gas fraction, and the time dependence is only due to the increasing gas fraction. To do this the viscosity at the lowest shear rate was fit with a curve as

shown on the figure. The minimum viscosity was assumed to be 3.5 Pa s, estimated from the initial viscosity measured here and the corresponding predictions using Equation 9.

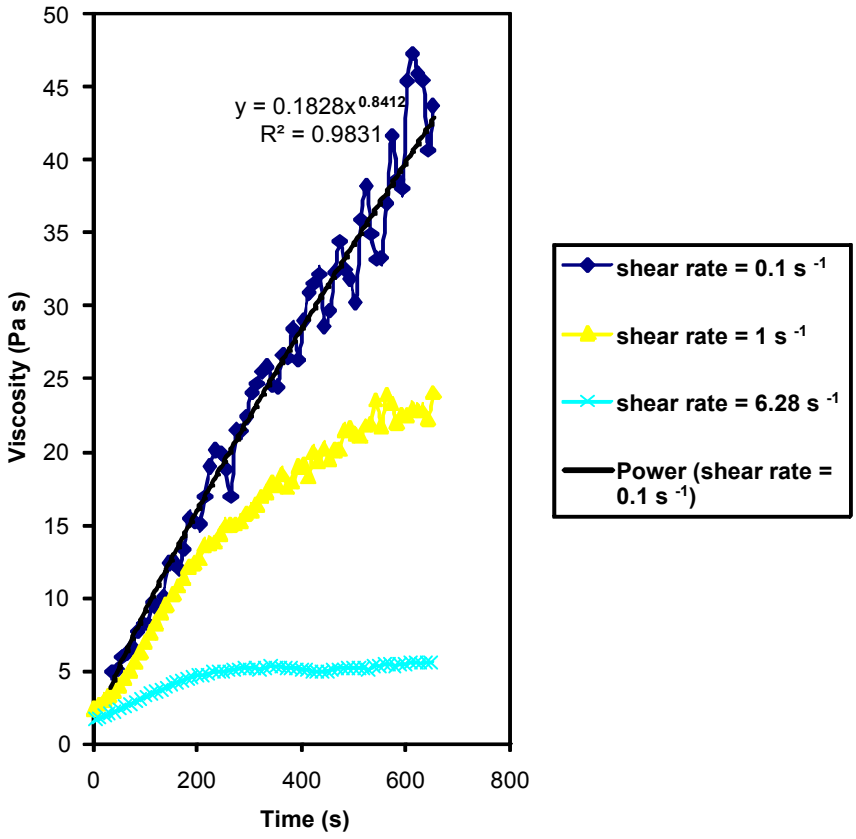

Figure 20. Parallel plate viscometry of evolving EFAR20 foam.

The gas fraction at each moment in time was estimated from the previous free-rise tests. The measured viscosity of the foam was compared to that predicted by Equation 10 and found to be adequate (Figure 21) for low shear rates. The comparison is excellent to a gas fraction greater than 0.5, the expected limit of this equation [Prud'homme and Khan 1995].

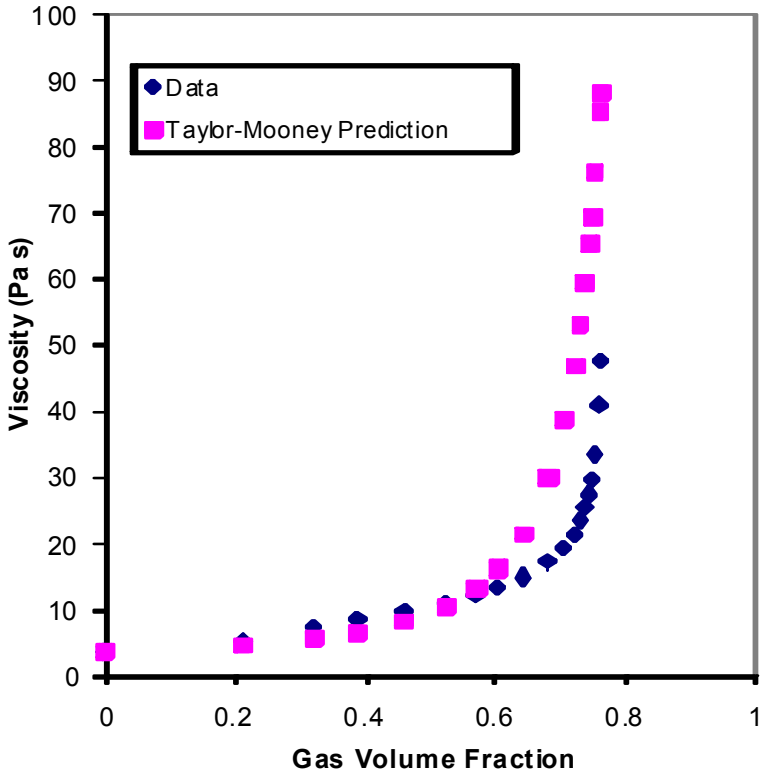

Figure 21. Foam viscosity as a function of gas content as measured (data) and as predicted by the Taylor-Mooney form derived from emulsion experiments (Prud'homme and Khan 1995).

3. BUBBLE NUCLEATION STUDIES

3.1. Single Droplet Experiments

Here we describe a series of experiments to study the nucleation physics of the blowing agent. Our goal was to determine what conditions are necessary for a drop of the blowing agent in liquid form to transform into a bubble of gaseous blowing agent.

In production, the foam is created by vigorously shaking to mix the blowing agent (Fluorinert™ FC-72) into the amine fraction of the epoxy. Since the blowing agent is immiscible in the epoxy, this mixing action disperses the blowing agent into a fine emulsion as well as incorporating many small air bubbles. Stabilizing agents, Dabco DC-193 surfactant and Cab-O-Sil M-5 (a fine silica aero-gel powder) are added to the amine fraction of the epoxy. Cab-O-Sil is also added as a nucleating aid and has been observed to enhance the foam rise. This mixture is then stirred into the epoxy resin, initiating the curing reaction, and placed into a preheated mold, initiating foaming. The blowing agent boils, generating bubbles that are trapped as the epoxy cures. The quality of the foam is characterized by the final rise of the foam or the final volume of the cured product.

The efficacy of the boiling nucleation process is critical to having a good rise, but the physics of the nucleation process are not well understood. This experimental study was designed to explore the conditions of nucleation more closely.

3.1.1. Pressure Cell

We have created an experimental capability to study isothermal nucleation carefully. By increasing the pressure over atmospheric, we can suppress boiling of the blowing agent until the temperature has equalized. By releasing the pressure, boiling can be rapidly initiated. The pressure cell designed for these experiments is shown in Figure 22. The body consists of a 7.6 cm (3”) OD, 5 cm (2”) ID acrylic glass cylinder held between aluminum end caps. Silicone gaskets seal the top and bottom of the cylinder. Locking washers are used on the stainless steel threaded rods that sandwich the pressure cell together, which helps it maintain tension on the cell when the temperature is raised (the thermal expansion of the metal is higher than the plastic). The top aluminum contains pass-throughs for the pressure control assembly and for a K-type thermocouple that records the temperature of the liquid inside of the cell. Reseating pressure relief valves (PRV) are used to control the pressure within a 5-psi range. The valve opens when the pressure becomes too high and then reseats once the excess pressure is vented. For the experiments discussed here, the maximum pressure was 50 psi, though this is adjustable.

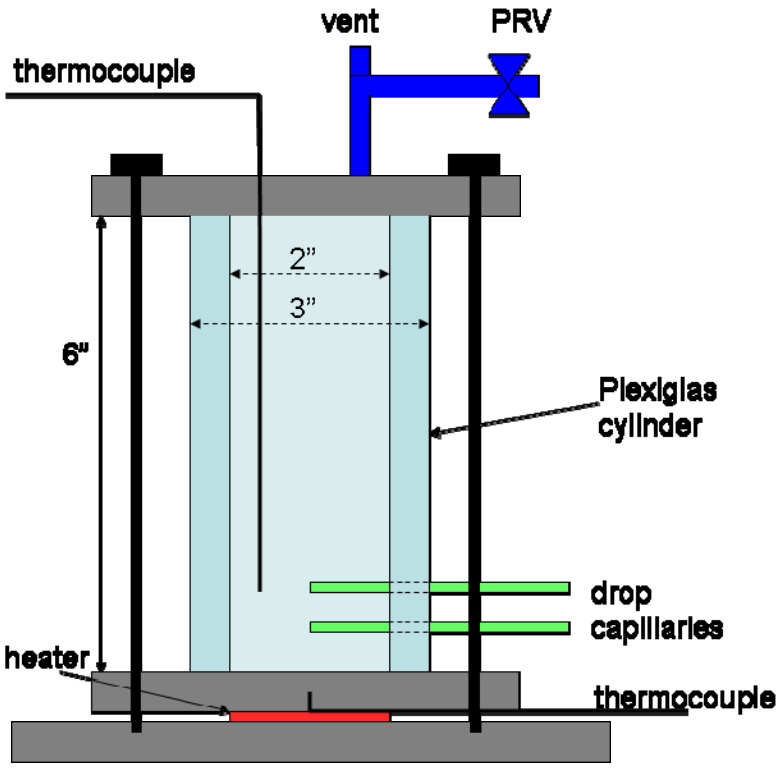

Figure 22. Pressure cell for nucleation studies.

The drops inside of the chamber are kept at the end of a 15 gauge stainless steel hypodermic needle tubing that connects directly to 0.16 cm (1/16") OD Swagelok pressure fittings. The capillary is connected to a low flow metering valve, both of which are completely filled with the fluid of interest. At the beginning of the test, the valve is positioned completely open, and, by closing the valve, fluid can be dispensed as drops through the tip of the capillary at both atmospheric and elevated pressure. Two capillaries were positioned 1.27 cm (½") and 2.54 cm (1") above the bottom of the cell respectively.

Once the test fluids were loaded into the cell, the chamber was brought up to pressure using compressed air and then heated to the desired temperature. A 5-cm (2") Kapton® heater was included in the base of the cell and regulated using a temperature controller based on a thermocouple that was potted into the floor of the pressure chamber. The entire cell was also placed inside a pre-heated oven. These two measures seemed to provide the best balance of heating speed and temperature uniformity. Typically temperature differences between the two thermocouples were less than 5°C and both were well above the boiling point of pure Fluorinert at sea level. Heating to a stable internal temperature required ~20-30 minutes, depending on the volume of fluid in the cell.

3.1.2. Fluorinert Nucleation Study

We performed three series of experiments in the pressure vessel to investigate the nucleation dynamics of Fluorinert in the curative part of the epoxy. The first looked at pure Fluorinert to

ensure that boiling would occur in the absence of the epoxy component. Then, drops of Fluorinert were examined isolated in the epoxy matrix. Finally, interactive Fluorinert and air drops were studied.

Figure 23 shows an experiment performed with pure Fluorinert in the cell. Initially 6 mL of Fluorinert were loaded into the bottom of the pressure chamber. The pressure was increased to 50 psi using house compressed air, then the vessel was disconnected and placed in an oven. Once the temperature of the bottom aluminum had stabilized at 68ºC, the pressure was released, dropping down to atmospheric pressure in no more than a few seconds. Almost immediately, the Fluorinert began to boil, presumably being nucleated from minor imperfections in the bottom machined aluminum surface.

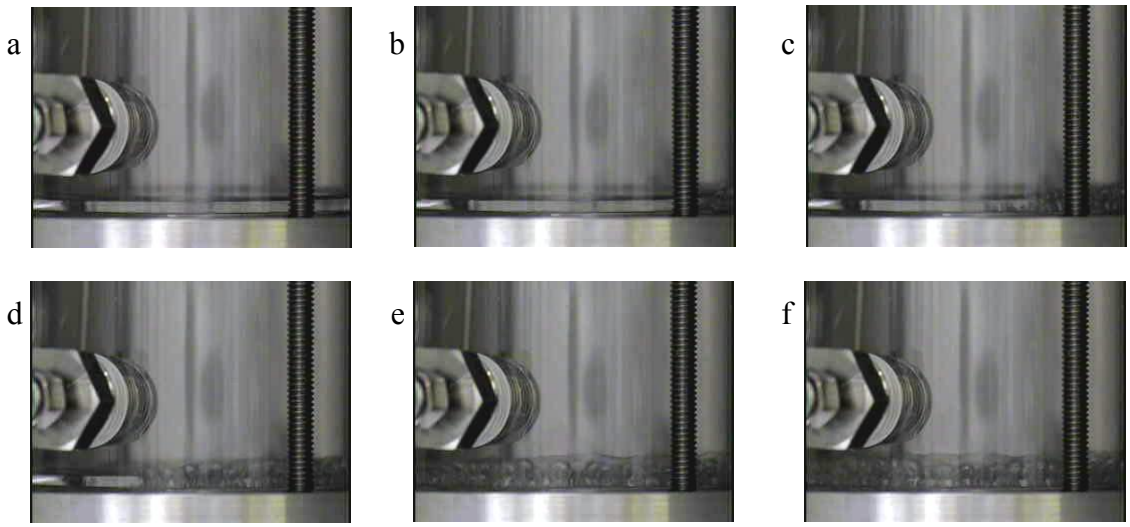

Figure 23. Experiment to test pressure cell with pure Fluorinert. Note bubbles forming on floor of chamber.

Next, to simulate the environment of a drop of Fluorinert in the epoxy, we employed our capillary injection ports to study the nucleation of a drop. We used only the curative portion of the epoxy mixture containing only the Ancamine and Epicure amines without any additives such as the Cab-O-Sil. Figure 24 shows the Fluorinert drop suspended in the amine matrix at an internal temperature of 58ºC. Once the pressure was released from the chamber, no nucleation was observed and the drop of Fluorinert was stable. Drops of Fluorinert that were left on the bottom of the smooth glass vessel were also stable and did not nucleate even at temperatures up to 70ºC.

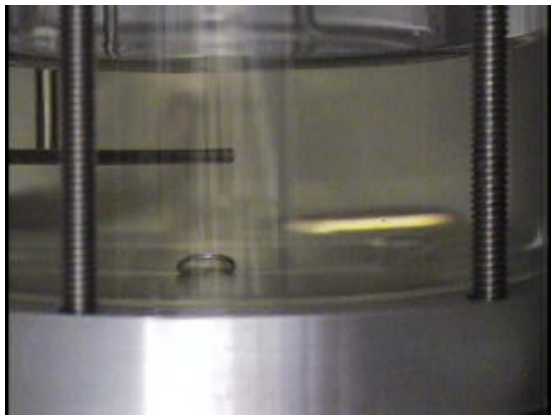

Figure 24. Stable drop of Fluorinert in curative matrix at atmospheric pressure.

3.1.3. Interaction Fluorinert and Air Bubbles

In the production of the foam mixture, there are suspended droplets of not only Fluorinert but also air introduced by the mixing process. One theory for the nucleation of the blowing agent is that heterogeneous nucleation by an air bubble is required. To test the potential importance of air bubbles in the nucleation process, we examined the interaction of Fluorinert and air bubbles in the curative matrix without Cab-O-Sil or surfactant.

For this experiment, the upper capillary was loaded with the Fluorinert blowing agent and the lower capillary was loaded with air. Once the temperature had stabilized and the pressure was released, the drops of air and Fluorinert could be expelled into the curative matrix where gravity would drive them towards each other. In many cases, the drops would roll over each other without causing a nucleation event. But, as shown below in Figure 25, the interaction of the two drops can also nucleate boiling of the Fluorinert.

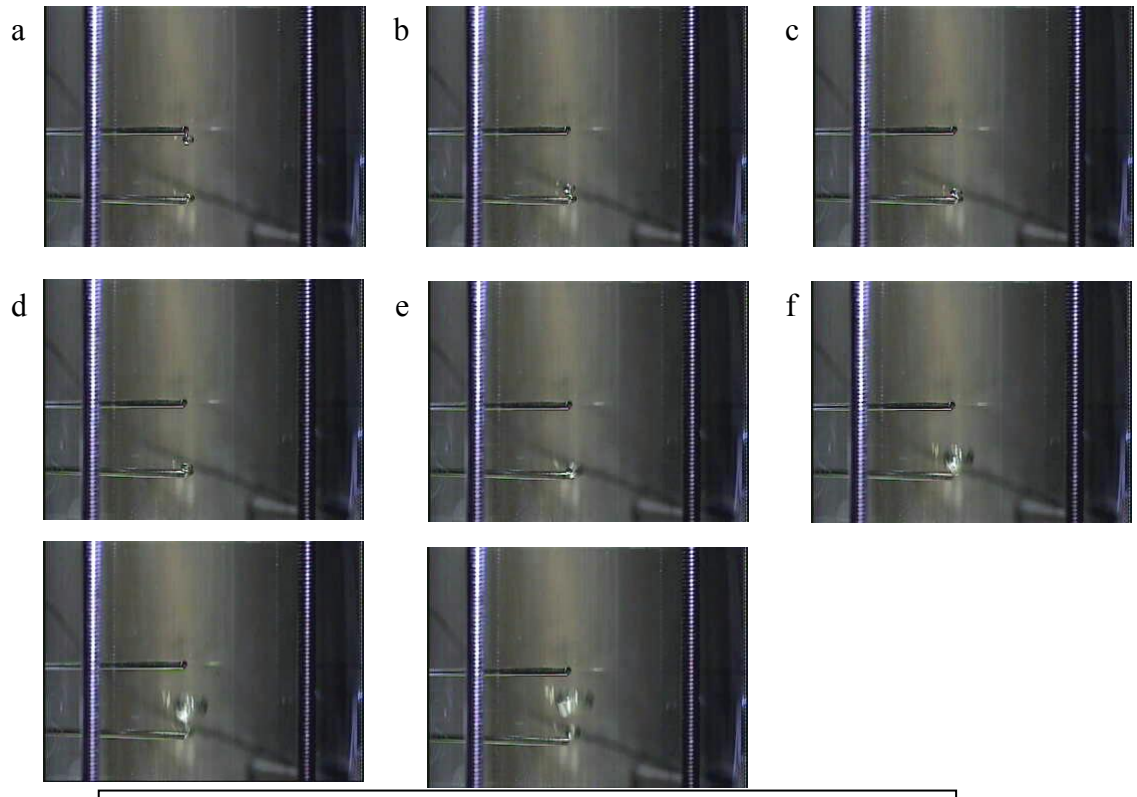

frames 76, 86, 87, 88, 89, 90, 112, 114
time 2.50 s, 2.84 s, 2.87 s, 2.90 s, 2.94 s, 2.97 s, 3.00 s, 3.04

Figure 25. Interaction of Fluorinert drop and air bubble resulting in nucleation event.

3.2. Additional Nucleation Experiments

Since our experiments in the pressure cell indicated that the Fluorinert blowing agent was stable to nucleation when marginally superheated, we decided to explore some simple experiments at atmospheric pressure to confirm the importance of air bubbles for heterogeneous nucleation of the blowing agent, as well as to explore both the role of the other additives to the curative and the potential for using another nucleating agent that would not be as process-dependent as air.

To test the effect of Cab-O-Sil on nucleation of the Fluorinert blowing agent, we heated a small glass jar containing the 'part B' curative mixture consisting of Ancamine, Epi-Cure, Cab-O-Sil and surfactant. Small drops of the Fluorinert were placed on the bottom of the jar in this solution. Unfortunately, due to the geometry of the jar used, the heating was very slow and primarily around the outer edge of the jar where it made contact with the heating element below. When the Fluorinert drops at the bottom edge of the jar were well above the boiling point, no nucleation occurred even in the solution containing Cab-O-Sil. However, if air bubbles were introduced manually with a syringe the Fluorinert could vaporize. Figure 26 shows the nucleation of one Fluorinert drop. The first frame (Figure 26a) shows a stream of bubbles which

failed to nucleate the drop, and then Figures 26b and c show the final successful nucleation event.

frames 40, 41, 42
times 1.20 s, 1.23 s, 1.27 s

Figure 26. Nucleation in curative matrix containing Cab-O-Sil and surfactant

To test the possibility of using another nucleating agent such as larger particles, and to improve the heating to be more uniform, we used a shallow, flat-bottomed, glass Petrie dish as our containing vessel in another set of experiments. First we introduced 400 grit sandpaper on the bottom of the dish. The sandpaper was rinsed with isopropanol and allowed to dry thoroughly. A half disk of the sandpaper was placed in the dish with the mixture of Ancamine and Epi-Cure curatives (sandpaper is on left side of the dish shown in Figure 27). Because of the viscosity of the curative mixture, it was difficult to get the sandpaper flat to the bottom of the Petrie dish, but the method was successful in preventing trapped air underneath the sand paper. Because of the rough surface of the sandpaper many tiny air bubbles were released after immersing in the curative mixture. Once the system seemed stable and no more additional air bubbles were released, Fluorinert drops were placed both on the sand paper and on the smooth glass surface of the Petrie dish as shown in Figure 27a; the red circles indicate the location of Fluorinert droplets.

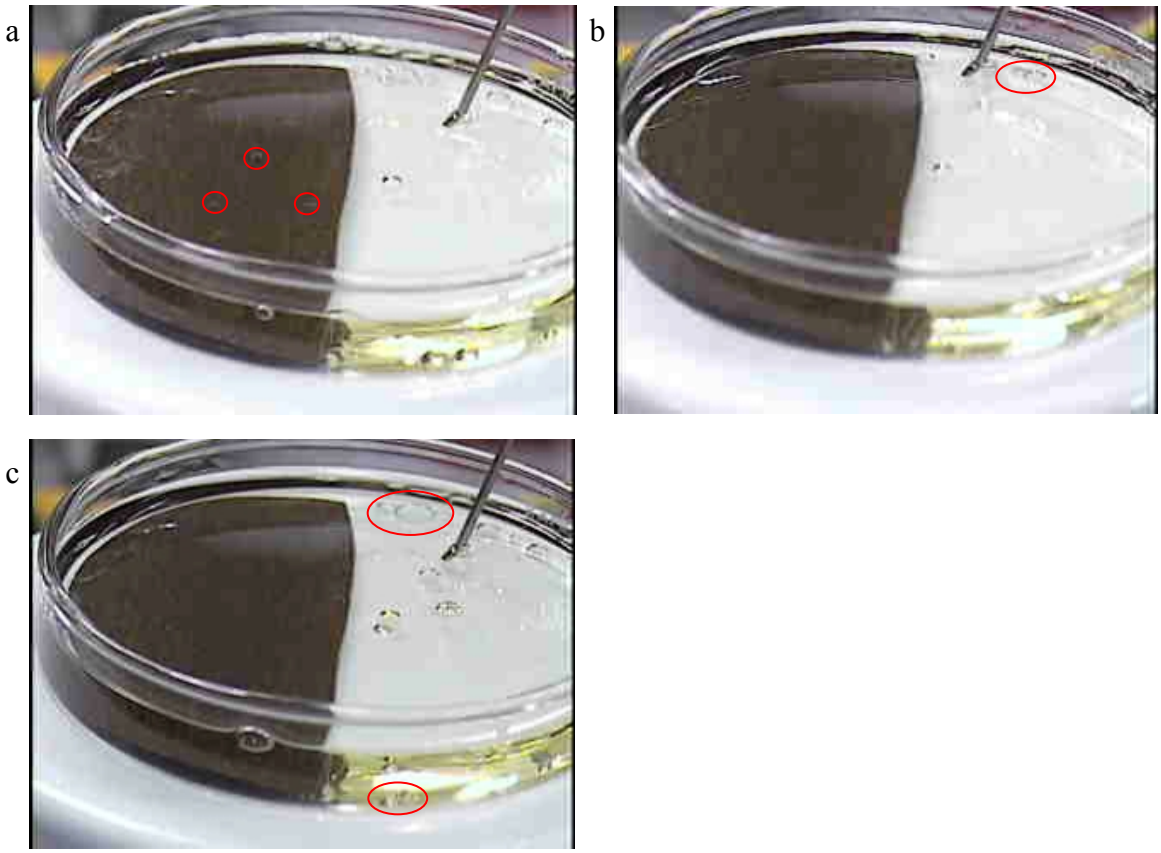

Figure 27. Effect of external nucleating agent on Fluorinert boiling.

When the temperature of the bottom of the Petrie dish reached 56ºC, the Fluorinert drops in contact with the sandpaper started to boil, with all of the drops boiling away by a temperature of 60ºC. Because of convection generated during heating the Fluorinert bubbles tended to migrate to the outer wall of the dish and coagulate to form bigger droplets. However, they did not boil on the plain glass surface (Figure 27b). Even as the temperature was above 75ºC, shown in Figure 27c, much of the Fluorinert on the glass side remained.

Next we attempted to form a more intimate contact between the Fluorinert and the Cab-O-Sil by mixing the Cab-O-Sil in the Fluorinert before injecting droplets into the curative mixture. We then tested this system in the Petrie dish without sandpaper. Some Fluorinert did boil, but only at temperatures higher than 65ºC, and again much Fluorinert remained above 75ºC. Finally, we tried larger particles, talc, estimated to be 5-10 μm in diameter. Again we mixed the particles into the Fluorinert phase, although the particles fell out of the droplets and onto the glass bottom during the experiment. Here, boiling began at approximately 56 ºC if the talc was introduced initially into the Fluorinert phase. If we only mixed the talc into the curative phase, boiling began at about 61 ºC.

3.3. Mixing Studies

Figure 28 illustrates that the final foam height of REF308 is influenced by the mixing method used to mix parts A and B [Gerding and Russick 2007]. Normally, part B is mixed with a paint shaker, which incorporates air bubbles, then the bubbly part B is mixed with part A. Here, the two parts of the foam were either mixed vigorously by hand or mixed with a four-blade propeller at 300 or 800 rpm. The resulting free rise density was 4.78, 5.35, or 4.6 pcf, respectively. Although not conclusive, photos taken of the initial mixture pressed between two slide plates seemed to show more bubbles present in the hand- and 800-rpm-mixed foams and fewer with the 300-rpm-mixed foam.

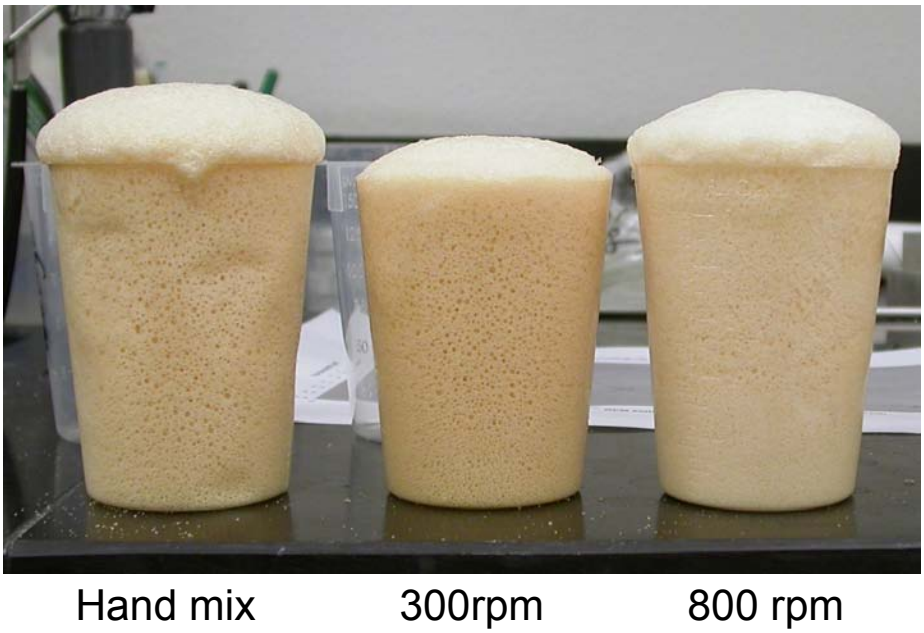

Figure 28. REF308 free rise foam created with various mixing methods for part B.

We carried these test further and looked at the effects of using a paint mixer not only to mix part B, but also to mix the two parts together. Figure 29 shows free rise EFAR08 (similar to EFAR20, but with a larger fraction of Fluorinert) foams created with traditional hand mixing and that formed after using a paint shaker and then sliced in half to show the inner structure. Figure 30 shows the slides of the initial epoxy mix before heating, corresponding to the foams in Figure 29. The slides seem to show more bubbles initially present in the machine-mixed foam and the corresponding foam is more homogeneous. The foam densities are virtually identical as seen by the height of the rise; however, the foam mixed exclusively with a paint shaker has finer cells. This is consistent with a foam formed with more nucleating sites for the same amount of blowing agent. Furthermore, no large cells occur in the center, unlike in the hand-mixed foam.

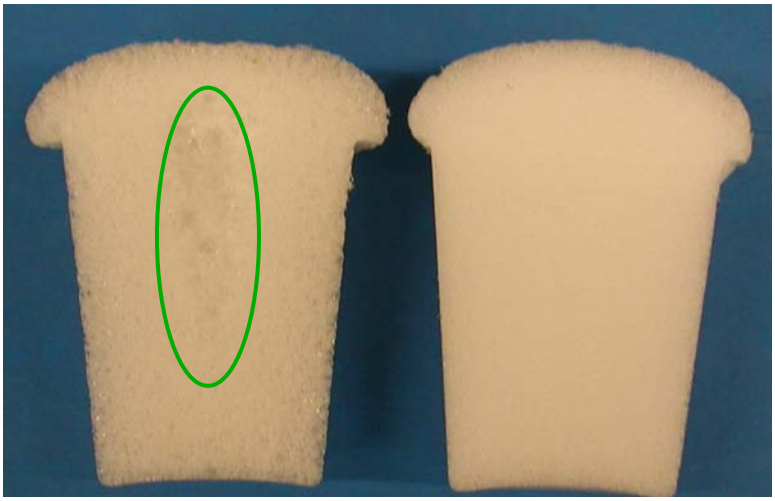

Paint shake Part B 30 min
Foam hand mix 1 min

Paint shake Part B 5 min
Foam paint shake 5 min

Figure 29. The effects of mixing on EFAR08.

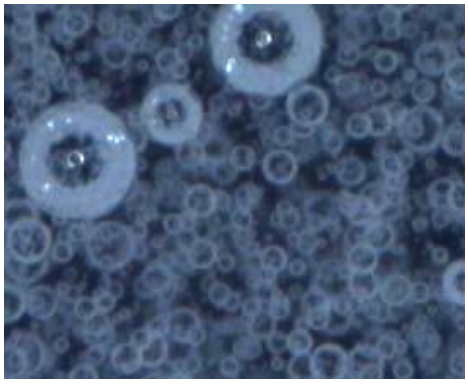

5-min paint-shake Part B
1-min hand-mix foam

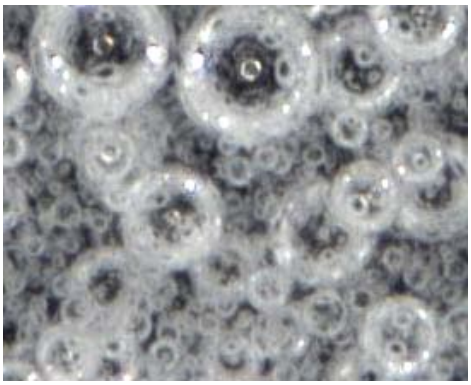

5-min paint-shake Part B
5-min paint-shake foam

Figure 30. Close up images of the initial epoxy mix in Figure 29 before heating.

4. EXPERIMENTS FOR VALIDATION OF MODEL

4.1. Flow Visualization of KC Mold

The Kansas City Plant, where they do the production encapsulation of firing sets for the W76-1, developed a quality assurance tool that is pictured in Figure 31. A complex channel is machined in an aluminum block and a clear acrylic cover is held on the front face with screws. To monitor the quality of the foam during an encapsulation process at Kansas City, this mold is filled with the foam encapsulant and monitored to make sure that it fills the part. Filling is through injection ports in the left hand corner of either the inner cup shape or the outer serpentine shape as shown in Figure 31. We took this mold, copied it, and instrumented it with four thermocouples. The first, thermocouple 101, is in the injection port machined through the back wall. It is not quite into the main reservoir. Thermocouples 102 and 103, are in the foam channel as pictured, about halfway between the front face of the back wall and the inner surface of the front cover and about halfway across the channel width. The fourth, 104, is within the mold itself, centered in the aluminum block about 0.16 cm (1/16 inch) from the inner face of the back wall, and so never touches foam.

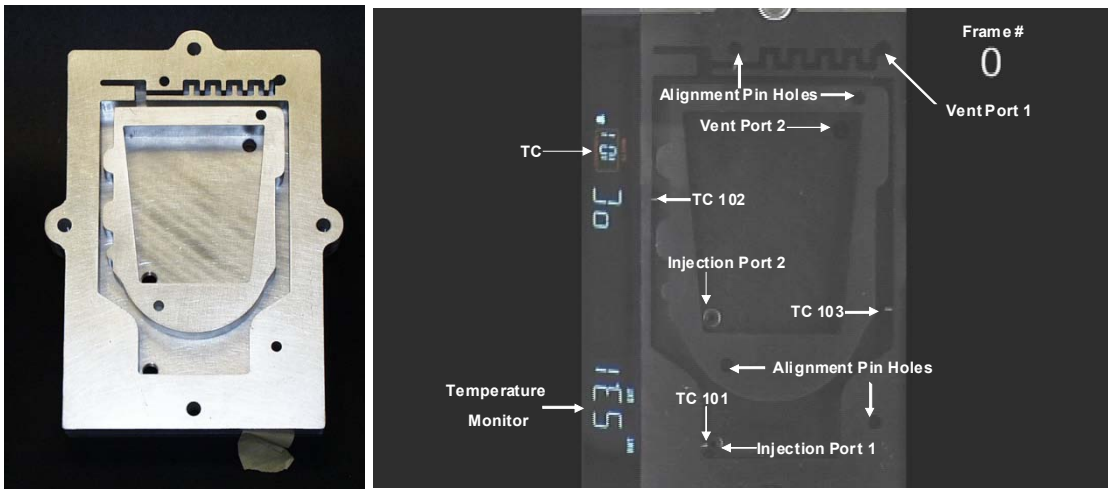

Figure 31. Kansas City mold (left), as seen in the videos and annotated (right).

The outer mold, consisting of narrow sections and serpentine routes for the foam to penetrate, was used for model validation studies. The inner cup was filled in the initial trials, but later ignored.

Foam was mixed with the same protocol as described in Section 2.1, and 20 g were injected into the bottom left corner of the mold. Laser flashes and synchronized voltage signals timed the injection and provided for a way to correlate the video films with the thermocouple measurements and time both from the initial mixing of parts A and B. Figure 32 shows a typical timing map.

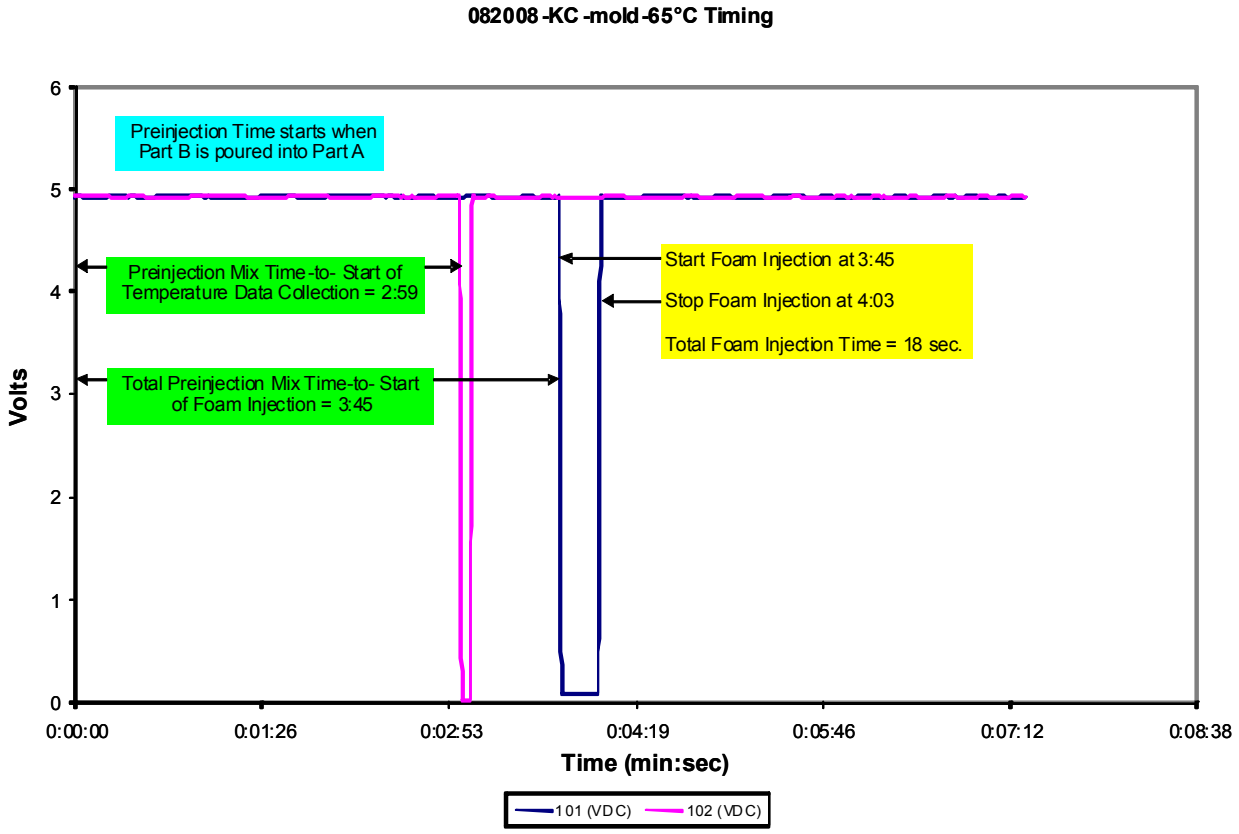

Figure 32. Time from mixing of Parts A and B to laser flashes labeling the video and synchronized voltage signals labeling the thermocouple measurements.

A series of frames from a video taken of a test with the oven at a nominal temperature of 65°C is shown in Figure 33. These can be used to validate the model against the shape and location of the leading fluid front with time. The frame stamp is in right top corner. Frame rate is 30 f/s.

The temperature shown on video (lower left, sideways) is being measured by thermocouple 101 in foam near the injection port near the bottom left of image. Here, we take time = 0 to be at the end of the injection, when the computational model starts. Foam hits the bottom of the inner curve at time = 10.43 s. At time = 58.10 s both arms of the foam hit the first corner on the inner wall, approximately the height of TC103 on the right side. By about 100 s the foam in the left channel has reached the level of TC102. The right channel fills faster than the left, and at time = 117.43 s the right arm has started around top corner. At time = 236.43 s the two arms just touch, and an arrow points just to the right of the knit line in Figure 33. By time = 337.07 s, foam has appeared in the right corner, seemingly spontaneously. This seems to be an experimental artifact, possibly caused by a leak in the front cover, although it may be that a large bubble has appeared between the upper right corner and the square wave section of the channel. Bubble

breakage was observed and may have led to that larger bubble. Also of interest is that a void appears at the dead-end on the upper left hand side of the mold (there is no vent in this corner), but disappears quickly either by leaking out of the mold or by diffusing into the foam.

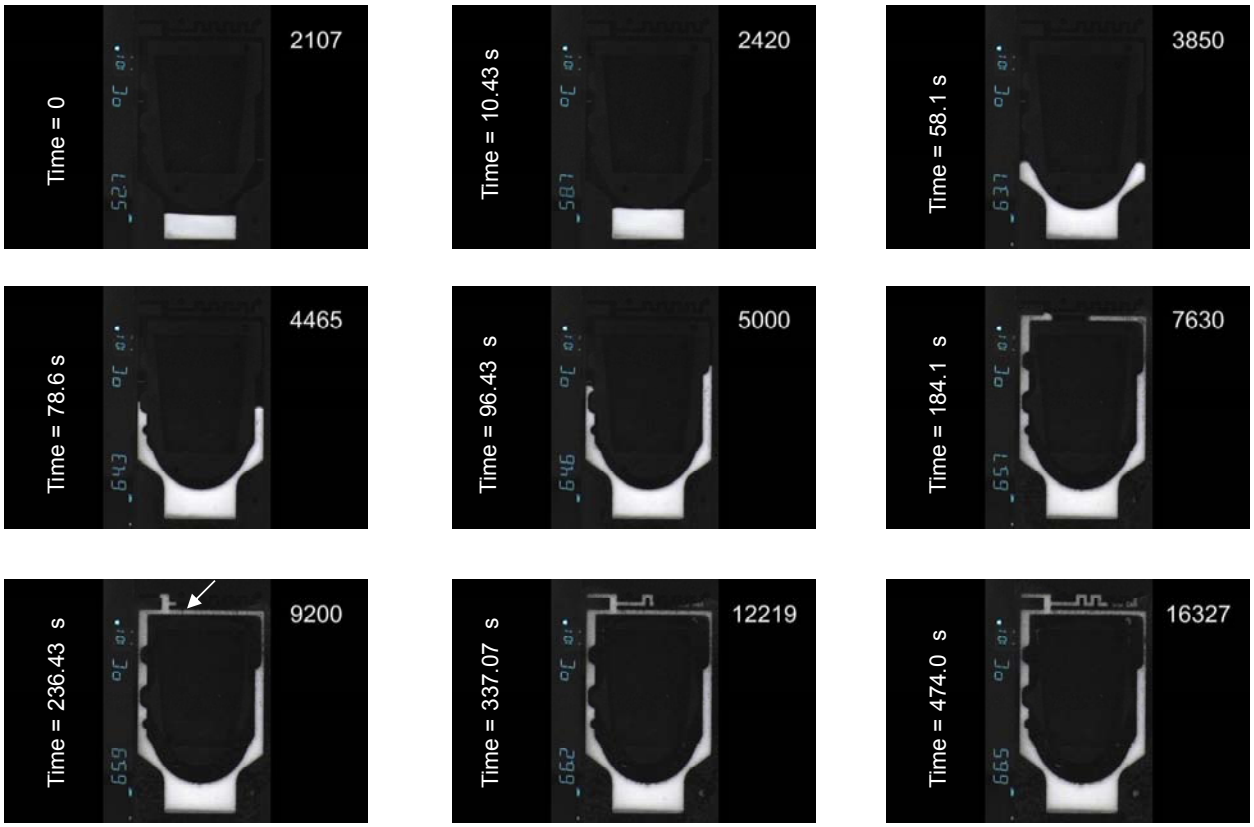

Figure 33. Series of frames from a movie of the filling of the mold in an oven with nominal temperature of 65°C.

With image processing, we determined the area of the fill for individual images, and knowing the depth of the channel and the time of each image, converted this to a fill rate in the form of volume of foam vs. time. The results are shown in Figure 34.

A repeat experiment was performed, and the results of the fill rate are also shown in Figure 34. The final foam in this repeat experiment had a finer texture, and there were no large voids in the thin regions. Looking at the final frame of both runs, the first one (06192008) had more un-blown epoxy at the bottom. Both have large bubbles which collected at the stagnation point at the bottom of the rounded part.

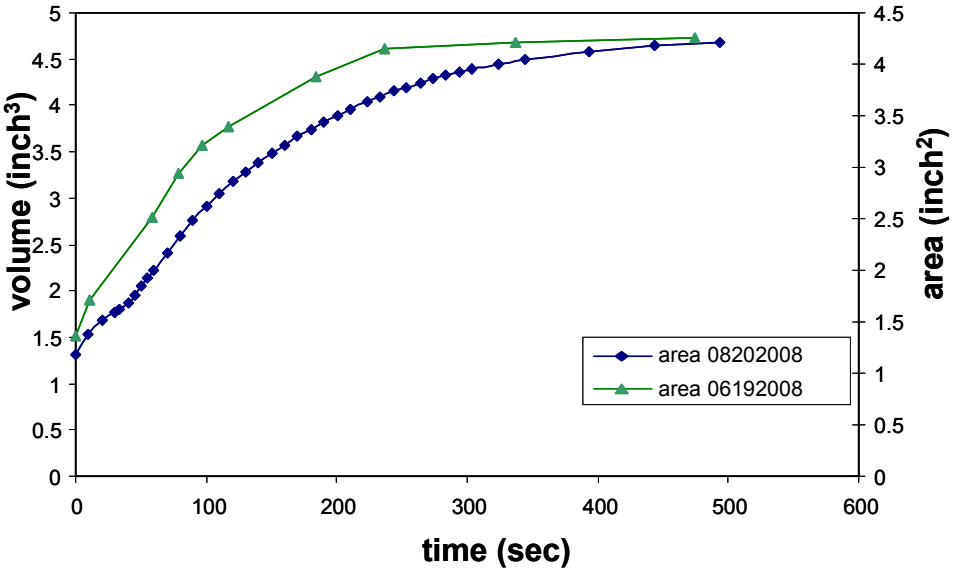

Figure 34. Volume of foam vs. time for test depicted in Figure 33 (06192008) and a later repeat (08202008).

4.2. Temperature Monitoring

Two nominal oven temperatures were tested: 53 and 65°C. Thermocouples were calibrated in a water bath against a calibrated thermister. The actual temperature based on the thermister readings are shown with the thermocouple readings in Figure 35. Subsequent to this calibration, and before the Kansas City mold studies, thermocouple 103 broke and was replaced with an uncalibrated thermocouple. The variations in the corrections among thermocouples were considered small enough to warrant using an average correction for the new thermocouple rather than calibrating again. One can see that the thermocouple reading were approximately 1°C lower than the actual temperature.

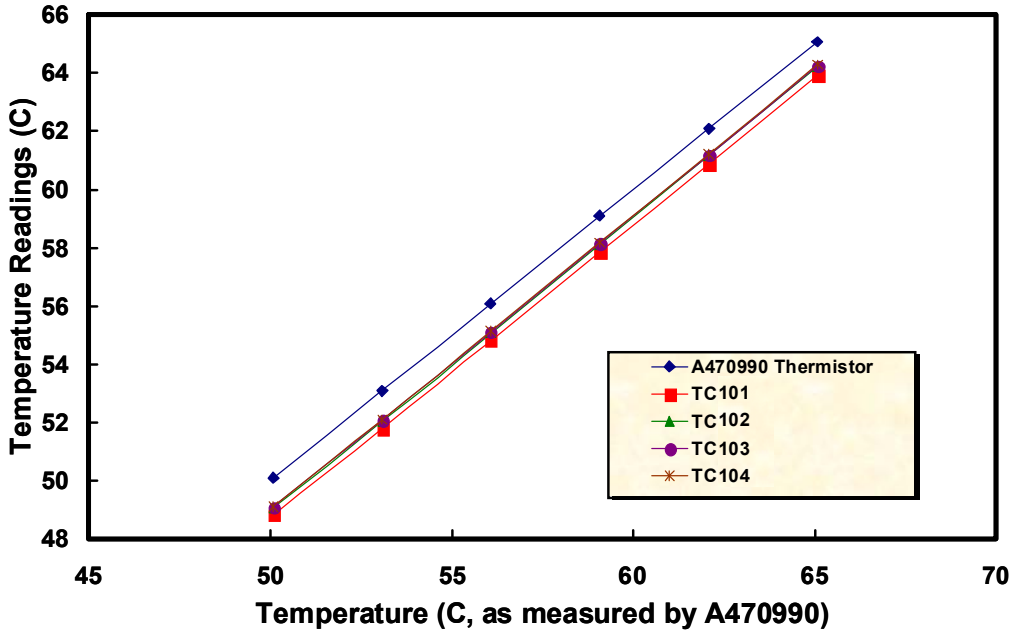

Figure 35. Calibration of thermocouples.

Figure 36 graphs the measured temperatures for the mold fill corresponding to Figures 33 and 34. The graph on the left displays all of the collected raw data. The graph on the right is corrected based on the calibration in Figure 35. It also shows the time shifted such that the initial time is now at the end of the injection period, based on the timing data shown in Figure 32. The thermocouple TC101 is located in the center of the inflow tube approximately flush with the back wall of the mold. When the cooler foam first enters the mold this thermocouple records the lowest reading. The material heats up some in the inlet tube from a mixing temperature of about 43 ^{o}C to the low reading of 52.7 ^{o}C. However, because this thermocouple is so close to the preheated aluminum walls of the inlet tube, after injection ends it is likely that the material left surrounding TC101 heats up more quickly to the mold temperature than the foam in the main reservoir. This seems to be the case, because when the foam reaches TC103, the reading dips about 2.5 ^{o}C from the air (oven/preheat) temperature, which is lower than the current reading given by TC101. TC102 is higher in the mold and the foam has had a chance to heat up more, so the reading changes little when the foam front hits this thermocouple. TC104 is embedded in the mold and stays almost constant throughout the experiment.

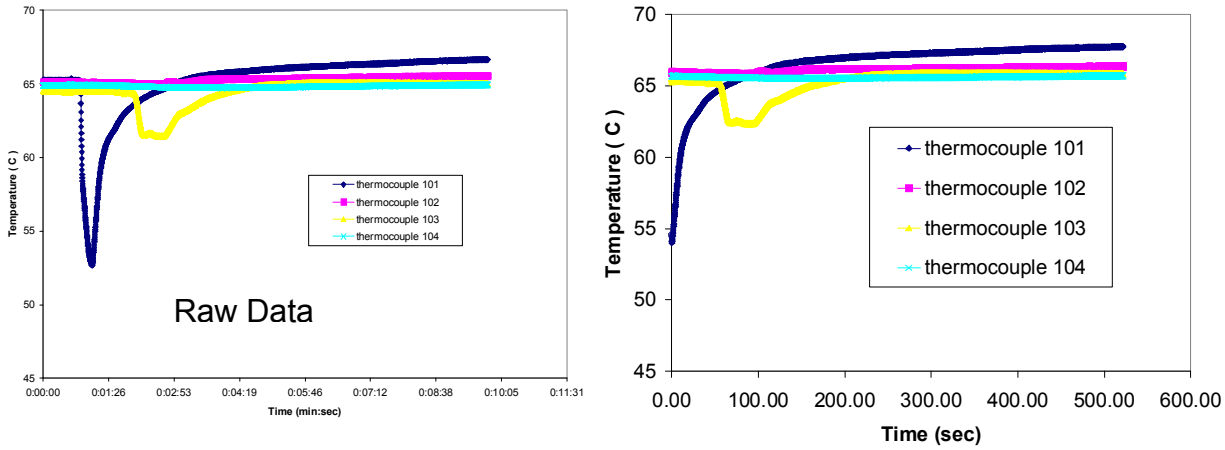

Figure 36. Temperature profile during KC mold fill.

4.3. X-ray CT

After the foaming process, the parts were cured in the oven. Afterwards, the parts were removed from the mold and analyzed with x-ray computed tomography (CT). The CT images were calibrated using a series of small foam samples whose average densities were determined by measuring the volume and mass. Figure 37 shows the calibration of intensity values with density in units of pounds per cubic foot (pcf), illustrating that the image intensity is directly proportional to the density.

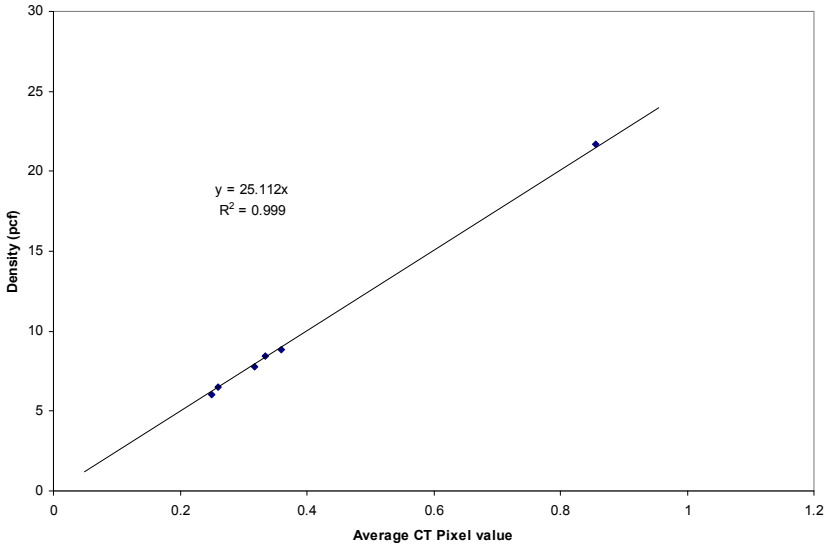

Figure 37. Calibration of x-ray CT image intensity based on 6 foam samples of known density.

Figures 38-40 show foamed parts (minus the square wave section at the top that was impossible to remove without breaking) for two different oven temperatures. The initial trials filling the KC mold often resulted in large voids and coarse-grained foam in narrow sections. Figure 38 shows foam inhomogeneities and a bright area at the bottom representing unfoamed material. Better "burping" of injection syringe improved the quality of subsequent tests (Figures 39-40). These difficulties highlight the sensitivity of the process and the sensitivity of the results to operator experience and skill.

Figures 38-40 include boxes indicating regions over which the image intensity values were averaged, and the density value corresponding to that average intensity. Density variations range from unfoamed (~1 g/cm^3) to foamed (0.2 g/cm^3), with foamed part varying approximately another 20%. A lower oven temperature slows foaming and filling of the part. Comparing Figures 39 and 40, one can see that the lower oven temperature results in a denser foam, but with a finer, more uniform cell structure, although the density gradients do not seem to be reduced. The narrowest section shows a more homogeneous foam and fewer large bubbles spanning the gap. Waiting about 30 seconds after mixing before injection changes the density and density gradients, but it is not clear whether this is just within the normal variations due to the intrinsic variability in the materials.

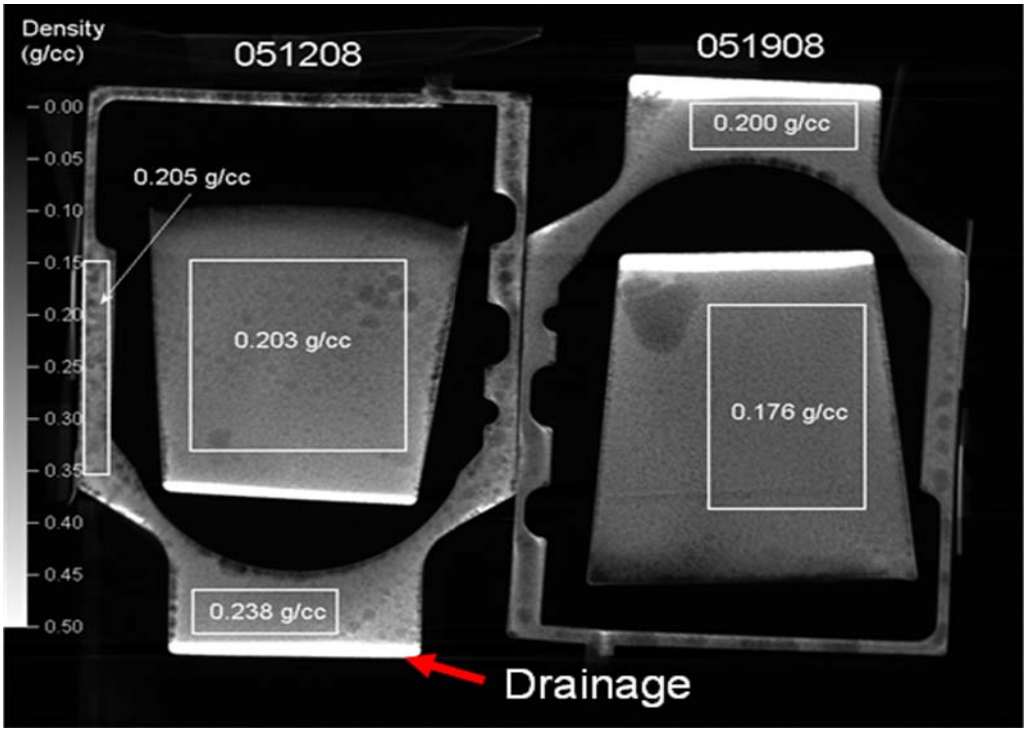

Figure 38. X-ray CT of two outer molds with a large free-rise cup associated with each. Density values are shown in grey scale and averages of boxed areas labeled separately. The figure on the right is upside-down.

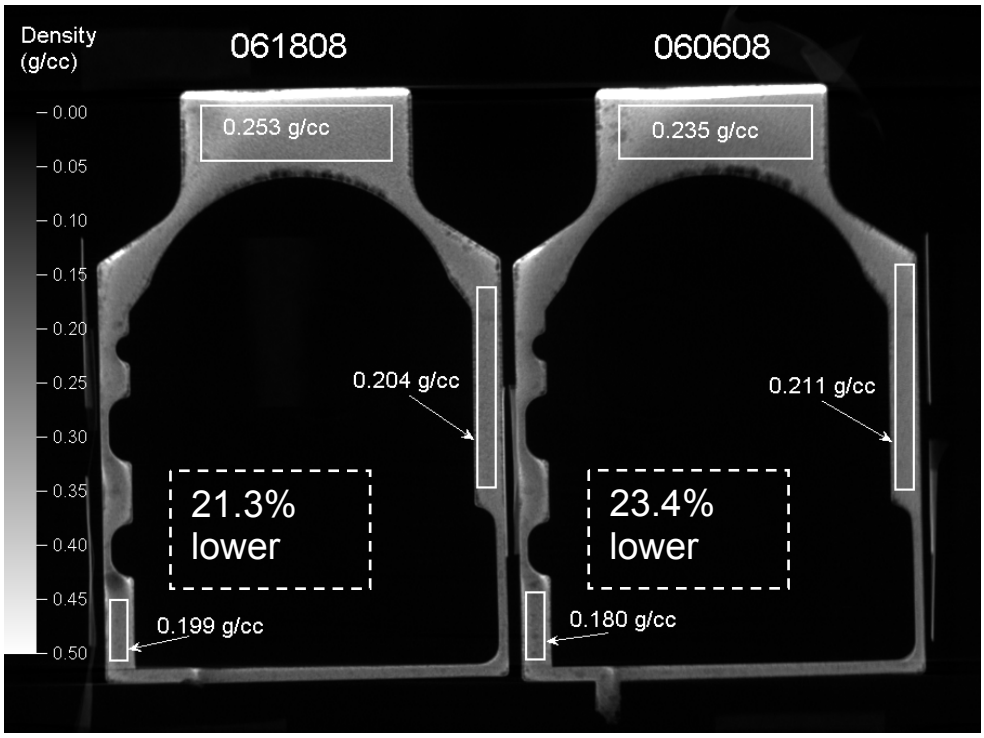

Figure 39. X-ray CT of two parts (upside-down) taken after more experience. Values in boxes outlined by a dotted line represent the difference between lowest and highest boxed regions.

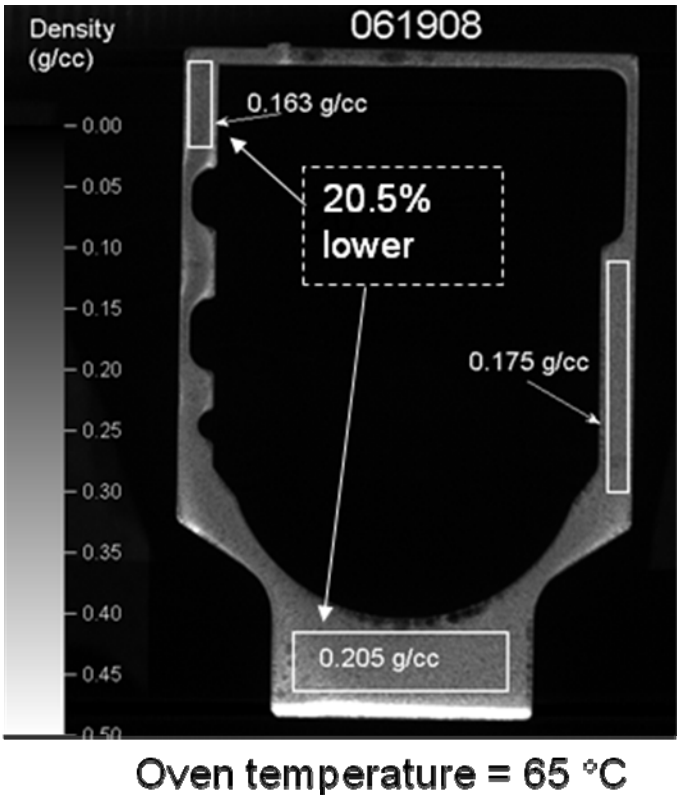

Figure 40. X-ray CT of a part taken after more experience. The value in the box outlined by a dotted line represents the difference between the lowest and highest boxed regions.

5. SUMMARY AND CONCLUSIONS

We have performed a series of experiments to provide information for the development of computational models of the process of foaming epoxy encapsulants. First, we have reported measurements of the changing density of EFAR20 and REF308 foam with time in free-rise experiments at various temperatures around the nominal oven temperature of the encapsulation process (65°C), and developed empirical density vs. time equations. We measure height vs. time and assume that the increase in height is solely from the increase in Fluorinert gas due to boiling. There is some uncertainty in the initial density of the foam because of incorporation of air, and this assumed density influences the interpretation of the results. However, the final density changes very little with the value assumed for the initial density. We recommend that the empirical fits (Equations 1 and 2) use the intrinsic density of the unfoamed epoxy (1.14 g/cm^3, in the case of EFAR20) and the final density of the part of interest. In the case of the KC mold experiments using EFAR20, the final foam density ranges from about 0.16 to 0.20 g/cm^3 at an oven temperature of 65^{o}C. However, for mass conservation, one must consider both the unblown foam at the bottom of the mold and that left in the injection line. In the case of our experiments the mold volume is 52.26 cm^3 and the volume of the injection line is 3.27 cm^3. The total mass injected is 20.0 g; therefore, the final overall average density of the part is 0.36 g/cm^3.

Second, the PIV results from this work show that our free rise foam has a slip velocity that occurs over a gas volume fraction range of 0.50 – 0.71. The presence of a slip velocity for foams within this volume fraction range agrees with theoretical predictions. The slip velocity profile consists of shear profiles near the perpendicular walls and plug flow profiles along the center. The shape of the slip velocity profile is consistent with non-curing foam systems [Calvert 1990, Calvert and Nezhati 1986, Kraynik 1988]. The decrease of the average slip velocity is the result of a decreased availability of the blowing agent and the increase in viscosity due to polymerization and increasing gas volume fraction. The slip coefficient was determined to be independent of foam viscosity and temperature when variations in foam materials are taken into consideration. The resulting slip coefficient is an order of magnitude smaller than those previously used. These data, in addition to the rise rate, density, and viscosity measurements will provide needed input to a finite-element-based computational model of free rise foaming being developed to aid in process optimization.

Third, we have measured the viscosity of the continuous phase, the viscosity of the foam, and the reaction kinetics of polymerization. From these measurements, we have developed equations for the foam viscosity based on the gas fraction, time, and extent of reaction (Equations 9 – 10). In addition, the heat of reaction was measured to be 250 J/g for EFAR20 and 134 J/g for REF308.

Fourth, our studies have shown the importance of air incorporation during mixing. If the epoxy mix sits too long before being placed in the oven, we observe separation of air bubbles to the top and settling of the Fluorinert to the bottom. This leads to a much denser foam after heating and to more unfoamed material at the bottom after curing. We have performed various simple tests to study the nucleation dynamics for Fluorinert FC-72 in EFAR epoxy. From the results, it is clear that air is an important nucleating agent in EFAR foams. Fluorinert droplets surrounded by the curative mixture did not boil even up to a temperature of 70 ºC. This indicates that the temperature for homogeneous nucleation is greater than 70 ºC , and that boiling in the

encapsulation process occurs through heterogeneous nucleation, requiring a nucleation site to initiate the change in phase. Cab-O-Sil mixed into the curative matrix does not seem to be effective in nucleating the Fluorinert droplets, but other nucleating agents such as sand paper may be effective. The hypothesis that incorporated air is the primary means of nucleation in the current process is consistent with tests of mixing methods, which show that using a paint shaker to mix the parts A and B together seems to result in a finer-celled foam, presumably because of more nucleation sites for a fixed amount of Fluorinert. Because of the higher quality, in terms of homogeneity, of the foams mixed with a paint shaker, we suggest that this practice be adopted into production.

Finally, we have provided code validation data in the forms of fill vs. time and temperature vs. time data. X-ray CT also provided density measurements of the final KC mold parts produced in a manner similar to the existing process at Kansas City. Significant density gradients exist, which do not appear to be a strong function of the oven temperature, although lowering the oven temperature did appear to minimize the formation of large bubbles in the narrow section at the top of the mold. Although beyond the scope of this work, we suggest that further studies be performed to examine this and to determine if using the paint shaker to mix parts A and B together would also minimize these density gradients.

6. REFERENCES

D. Adolf, 1996, Measurement Techniques for Evaluating Encapsulant Thermophysical Properties During Cure, Sandia National Laboratories, SAND096-1458.

D. Adolf, J. Martin, R. Chambers, S. Burchett, and T. Guess, 1997a, Stresses During Thermoset Cure, Sandia National Laboratories, SAND097-0692J.

D. Adolf, R. Strommen, and H. Johnson, 1997b, Viscosity of Epoxy Encapsulants, Sandia National Laboratories, SAND097-2631.

J.R. Calvert, 1990, "Pressure Drop for Foam Flow through Pipes," *Int. J. Heat and Fluid Flow* **11**(3), 236-241.

J.R. Calvert and K. Nezhati, 1986, "A Rheological Model for a Liquid-Gas Foam," *Int. J. Heat and Fluid Flow* **7**(3), 164-168.

J.D. Ferry, 1980, *Viscoelastic Properties of Polymers*, Wiley, NY, p. 290.

M. Gerding and E. Russick, 2007, personal communication.

A.M. Kraynik, 1988, "Foam Flows," *Ann. Rev. Fluid Mech*. **20**, 325-357.

J.P. Martin, D.B. Adolf, and J.P. Wilcoxon, 1989, "Viscoelasticity Near the Sol-Gel Transition," *Physical Review A* **39**: 1325-1332.

R.K. Prud'homme and S.A. Khan, 1995, "Experimental Results on Foam Rheology," in *Foams: Theory, Measurements and Applications*, Prud'homme and Khan, Eds., Surfactant Science Series, V. 57, Marcel Dekker, Inc., New York, p. 234.

D. Seo and Y.R. Youn, 2005, "Numerical Analysis on Reaction Injection Molding of Polyurethane Foam by using a Finite Volume Method," Polymer 46(17), 6482-6493.

R. Sulo, S. Eick, and R. Grossman, 2005, "DaVis: A tool for Visualizing Data Quality." Available at: http://www.rgrossman.com/dl/proc-095.pdf

DISTRIBUTION

4 James Mahoney
Advanced Engineering Simulation and Analysis
Honeywell Federal Manufacturing and Technologies, Kansas City Plant
P.O. Box 419159
Kansas City, Missouri 64141-6159

1	MS0346	Christopher Brotherton	1513	
1	MS0346	Christopher Bourdon	1513	
1	MS0346	Anne Grillet	1513	
1	MS0346	Allen Gorby	1513	
3	MS0346	Lisa Mondy	1514	
1	MS0346	Dan Rader	1513	
1	MS0557	Sarah Leming	1521	
1	MS0555	Chris O'Gorman	1522	
1	MS0555	Kyle Thompson	1522	
1	MS0776	James Schreiber	6782	
1	MS0826	Jaime Castañeda	1512	
1	MS0826	Raymond Cote	1512	
1	MS0826	Mike Valley	1512	
1	MS0836	Terry Aselage	1514	
1	MS0836	Andrew Kraynik	1514	
1	MS0836	Harry Moffat	1514	
2	MS0836	Rekha Rao	1514	
1	MS0886	James Aubert	1821	
1	MS0888	Edward Russick	1821	
1	MS0958	Mike Kelly	2453	
1	MS1064	Marc Polosky	2614	
1	MS1245	Douglas Adolf	2453	
1	MS0899	Technical Library	9536	(electronic copy)


Sandia National Laboratories